NTNU

Norwegian University of
Science and Technology

Real-Time Hybrid Model Testing

Force-actuation and implementation

Vegard Rørvik Solum

Marine Technology

Submission date: June 2017

Supervisor: Roger Skjetne, IMT

Co-supervisor: Valentin Chabaud, IMT
Thomas Sauder, IMT
Einar Ueland, IMT

Norwegian University of Science and Technology

Department of Marine Technology

Abstract

Real-time hybrid model testing: Force-actuation and implementation

To be able to understand the behaviour of complex mechanical systems, physical testing has been - and still is - of importance. Sophisticated models and numerical tools have been developed to analyze the dynamics of such systems, but still some physical phenomena are not yet fully understood. These uncertain phenomena must be studied by physical testing - usually in model scale. However, physical testing also has its limitations. Difficulties due to scaling effects or restrictions of the testing facilities can be mentioned. Real-time hybrid testing is a name given to testing methods that combine physical tests in model scale, with numerical simulations of a system part. The concept has the potential of enhancing convenience and reducing cost. Real-time hybrid testing is based on dividing complex structures into two system parts: one that is physically tested and one that is simulated numerically. The two system parts interact in real time through a network of sensors, computations and actuators. The idea is to establish a system emulation that exploits the advantages of numerical simulations, while still capturing the most uncertain physical phenomena by physical tests.

The thesis presents the design of a force-actuation system for use in real-time hybrid testing. The system will be used to actuate the response of a numerical substructure on a physical substructure in an emulation of a coupled mass-spring-damper system. The force-actuation system consists of a position-controlled DC-servomotor in combination with a compliant element, a wheel and a wire. When trying to control forces on a moving object, different challenges arise. The thesis aims at clarifying some of these challenges. It is observed that time delays introduce extra damping to the system, and a compensation method based on polynomial prediction is proposed and analyzed. Performance of the force-actuation system is improved by the use of a predictor, but it does not eliminate the problem entirely. With limited performance of the force-actuator, it will be difficult to establish a valid real-time hybrid test since some frequencies are not reconstructed properly in the test.

SAMMENDRAG

For å kunne forstå oppførselen til komplekse dynamiske system, har fysisk testing vært viktig. Sofistikerte modeller og numeriske verktøy har blitt utviklet for å kunne analysere dynamikken til slike system, men fortsatt er enkelte fenomen uavklarte. Slike fenomen må fortsatt analyseres ved fysisk testing - vanligvis i modellskala. Fysisk testing har imidlertid også sine begrensninger. Vanskeligheter relatert til skaleringseffekter eller restriksjoner ved testområdet kan bli nevnt. Testmetoder som kombinerer fysiske tester i modellskala med numeriske simuleringer av et delsystem omtales som sanntid hybrid modelltesting. Konseptet har potensial til å øke anvendelighet og redusere kostnader ved testing. Sanntid hybrid modelltesting baserer seg på å dele komplekse system opp i to systemdeler: ett som testes fysisk og ett som simuleres numerisk. Det vil være sanntids interaksjon mellom systemdelene, gjennom et nettverk av sensorer, matematiske beregninger og responsaktueringer. Idéen er å opprette en systemetterligning som utnytter fordelene ved numerisk simulering, men fortsatt hensyntar noen fenomen gjennom fysiske tester.

Denne avhandlingen presenterer design og utvikling av et kraftaktueringssystem for bruk i sanntid hybrid testing. Systemet vil bli brukt til å påføre responsen av en numerisk systemdel på en fysisk systemdel i en etterligning av et koblet masse-fjærsystem. Kraftaktueringssystemet består av en posisjonskontrollert DC-servomotor i kombinasjon med en elastisk klokkefjær, et hjul og en wire. Når vi prøver å påføre krefter på et objekt i bevegelse, oppstår utfordringer. I avhandlingen blir noen av disse utfordringene diskutert. Det er observert at tidsforsinkelser introduserer ekstra demping til systemet, og en kompensasjonsmetode basert på polynom-prediksjon er beskrevet og analysert. Kraftaktueringssystemet gir bedre resulteter ved bruk av prediksjon, men dette fjerner ikke problemet helt. Med begrenset ytelse av kraftaktueringssystemet, vil det være vanskelig å etablere en godkjent sanntid hybrid test, siden enkelte frekvenser ikke blir rekonstruert i testen.

Preface

This thesis present the work done in the final part of the Master of Science degree in Marine Technology at the Norwegian University of Science and Technology, with specialization in Marine Control Engineering. The thesis was written during the spring of 2017, and is a continuation of the work done in a project thesis of fall of 2016. The work has been carried out in collaboration with candidate Truls Hamland, and the thesis presents the combined contributions with emphasis on what has been responsibility of Vegard R. Solum. The overall work load of the master thesis should be equivalent to 30 ECTS.

The thesis presents the design of real-time hybrid model tests, and aims at providing more information on the topic. Focus has been on developing a force-actuation system for use in testing.

Several people have been helping me throughout the work on this thesis. I am grateful for their guidance and useful ideas. First of all, I would like to thank my supervisor, professor Roger Skjetne for keeping me on the right track and providing me with useful help when needed. Furthermore, I would like to thank my co-advisors for guidance and valuable discussions, helping me obtain the results I did. PhD Valentin Chabaud, PhD candidate Einar Ueland, PhD candidate Thomas Sauder and PhD candidate Stefan Vilsen have been supportive and great sources of knowledge for me in this field of work. For a period of time I have had the pleasure of sharing laboratory/office with Valentin Chabuad and Einar Ueland. During that period, their experience has been highly valuable to me in my work. I am also thankful to senior engineer Torgeir Wahl at NTNU for essential help with implementation of hardware and communication between units. His help has spared me for a lot of laboratory time and headaches, and he made the development of a real-time hybrid test setup possible.

Trondheim, June 24, 2017

NTNU Trondheim
Norwegian University of Science and Technology
Department of Marine Technology

MSC THESIS DESCRIPTION SHEET

Name of the candidate: Vegard Solum
Field of study: Marine control engineering
Thesis title (Norwegian): Sanntid hybrid modelltesting: Kraft-aktuering og implementasjon
Thesis title (English): Real-time hybrid model testing: Force-actuation and implementation

Background

Real-time hybrid model (or ReaTHM™, as trademarked by Sintef Ocean) testing is the name given to the real-time coupling of experimental (here in the field of marine hydrodynamics) and numerical methods. It is a subclass of the well-known hardware-in-the-loop (HIL) testing, aiming at simulating and actuating secondary processes instead of modelling them physically (or even not including them) in hydrodynamic model tests.
This method has been successfully applied by Sintef Ocean and NTNU to the real-time actuation of wind loads on a floating wind turbine structure subjected to hydrodynamic loading, based on online motion measurements. A research project to further develop this method is ongoing.

The development of force-controlled linear actuators based on position-controlled servomotors has been a central task, and necessitates further improvements. The current solution consists of a torsion spring connected to the motor on one side and to a pulley on the other side, the latter pulling on a pretensioned wire to achieve linear force control. The force observer and controller currently implemented are exceedingly simple and tuned mostly based on trial-and-error. Particular issues related to inaccuracies in the observer and excitation of eigenmodes of the structure that the actuator is connected to, must be addressed. These issues may be related to time delays, which are inherent in ReaTHM™ testing.

From this arises the need for system identification of the actuation system, to be used for model-based design (e.g. optimal state estimation/control methods), and applied to the current force actuation setup.

Any HIL setup should in practice be thoroughly verified numerically. A real-time communication is set up with Sintef Ocean's software SIMA, which is able to model in high fidelity both the physical substructure (the system under study) and the actuator system. This highly flexible tool can be used for applying the designed control system on a realistic marine application.

Work description

1) Perform a background and literature review to provide information and relevant references on:
    - Force-based and displacement-based real-time hybrid testing.
    - Force actuation system and components.
    - Challenges of force-based real-time hybrid model testing in marine hydrodynamic applications.
        - Flexible modes in force actuation system and physical substructure.
        - Collocated vs non-collocated force control and allocation.
        - Time-delay linear systems: Modeling, identification, stability and compensation.
        - Combined force tracking and damping on elastic structures.
        - Feedforward and feedback control mechanisms.
    - Measurements and communication.
    - Observer designs.
    - Role of predictor function.

    Write a list with abbreviations and definitions of terms, explaining relevant concepts related to the literature study and project assignment.

2) Perform (together with Truls Hamland) a "from scratch design" of a force-based real-time hybrid model test setup:
    a) Mass-spring system (flexible regarding system properties such as stiffness and mass).
    b) Acquire the necessary components for force-actuation, position measurements, force measurements, etc.

c) LabVIEW and CompactRIO. Become familiar with the software and hardware to be used, and establish communication between units.
d) Specify a baseline test plant, to be used as a reference for the analysis as explained in point 3) below.
e) Design the force-based control system, with specific responsibility of the entire hybrid test loop. Some important system components will be:
   i) Physical/numerical substructuring.
   ii) Position observer design.
   iii) Loop delays and prediction.
   iv) Numeric simulation.
f) Specify relevant KPIs (Key Performance Indicators) and benchmark load cases (decay tests, chirp excitation, etc.) for testing and comparison of performance of the different components.
g) Perform model identification tests.

3) Perform an experimental verification and validation of the system:
   a) Verify that the force actuation system developed in 2) is able to apply forces of right amplitudes and frequencies.
   b) Study the KPIs and their sensitivity to parametric variations.
   c) Do a verification of the system based on replacing the baseline test plant with the hybrid substructures and the force actuation system.

Specifications

The scope of work may prove to be larger than initially anticipated. By the approval from the supervisor, described topics may be deleted or reduced in extent without consequences with regard to grading.

The candidate shall present personal contribution to the resolution of problems within the scope of work. Theories and conclusions should be based on mathematical derivations and logic reasoning identifying the various steps in the deduction.

The report shall be organized in a logical structure to give a clear exposition of background, results, assessments, and conclusions. The text should be brief and to the point, with a clear language. Rigorous mathematical deductions and illustrating figures are preferred over lengthy textual descriptions. The report shall have font size 11 pts. It shall be written in English (preferably US) and contain the following elements: Title page, abstract, acknowledgements, thesis specification, list of symbols and acronyms, table of contents, introduction with objective, background, and scope and delimitations, main body with problem formulations, derivations/developments and results, conclusions with recommendations for further work, references, and optional appendices. All figures, tables, and equations shall be numerated. The original contribution of the candidate and material taken from other sources shall be clearly identified. Work from other sources shall be properly acknowledged using quotations and a Harvard citation style (e.g. *natbib* Latex package). The work is expected to be conducted in an honest and ethical manner, without any sort of plagiarism and misconduct. Such practice is taken very seriously by the university and will have consequences. NTNU can use the results freely in research and teaching by proper referencing, unless otherwise agreed upon.

The thesis shall be submitted with a printed and electronic copy to the main supervisor, with the printed copy signed by the candidate. The final revised version of this thesis description must be included. The report must be submitted according to NTNU procedures. Computer code, pictures, videos, data series, and a PDF version of the report shall be included electronically with all submitted versions.

Start date: 15 January, 2017 **Due date:** As specified by the administration.

Supervisor: Roger Skjetne
Co-advisor(s): Valentin Chabaud, Einar Ueland, Thomas Sauder, Stefan Vilsen.

Trondheim,

_____

Roger Skjetne, Supervisor

Contents

Nomenclature

Acronym	Description
ReaTHM^{TM} test	Real-Time Hybrid Model test (trademarked by Sintef Ocean)
HIL	Hardware-in-the-loop
MIL	Model-in-the-loop
KPI	Key Performance Indicator
DOF	Degree-of-freedom
LabVIEW	Laboratory Virtual Instrument Engineering Workbench
NI	National Instruments
FPGA	Field-programmable gate arrey
PID	Proportional-Integral-Derivative control
BIBO	Bounded-input bounded-output
DDE	Delay-differential equation
PSD	Power spectral density
MSE	Mean-squared error

Symbol	Description
m	Mass
k	Stiffness constant
b	Damping constant
$\ddot{x}$	Linear acceleration
$\dot{x}$	Linear velocity
x	Linear position
m_P	Mass of physical substructure
k_P	Stiffness constant of physical substructure
b_P	Damping constant of physical substructure
m_N	Mass of numerical substructure
k_N	Stiffness constant of numerical substructure
b_N	Damping constant of numerical substructure
F	Force
F_{ext}	External force
$F_{ext,N}$	External force subjecting numerical substructure
$F_{ext,P}$	External force subjecting physical substructure
F_N	Force induced by numerical substructure onto physical substructure
F_P	Force induced by physical substructure onto numerical substructure
Δt	Time increment
θ_M	Motor angle
θ_w	Wheel angle
k_s	Clock-spring stiffness
r	Radius of wheel
$\theta_{M,ref}$	Force controller output, motor controller reference angle
F_m	Measured force
$\hat{x}$	Estimated position
F	Wheel angle
O_{wheel}	Circumference of wheel
$O_{encoder}$	Circumference of encoder
V	Voltage
F_{ref}	Reference force
e	Error between reference force and applied force
K_p	Proportional gain
K_i	Integral gain
K_d	Derivative gain

Symbol	Description
h_{eq}	Equivalent pure time delay
ϕ	Phase
h	Pure time delay
ω	Circular frequency in [rad/s]
f	Frequency in [Hz] or function
H	Transfer function
y_m	Measured output
H	Transfer function
j	Imaginary number
ω_c	Crossover frequency
ω_{180}	Frequency at which phase cross -180 degrees
T	Sampling period
n	Degree of polynomial
p_n	Polynomial of degree n
j	Imaginary number
m	Number of sampling points of polynomial interpolation
F_0	Pretension
ζ	Damping ratio
ω_0	Natural circular frequency
f_0	Natural frequency
ζ_P	Physical substructure damping ratio
θ_{th}	Force analytical estimate
$L(s)$	Lowpass filter in Laplace domain
b	Bias
$\dot{b}$	Bias derivative
$\hat{b}$	Bias estimate
w_b	White noise
$\hat{y}$	Estimated output
θ_{us}	Ultra sound wheel angle measuremant
θ_e	Encoder wheel angle measurement

Chapter 1

Introduction

1.1 Background

Real-time hybrid model testing is a name given to the real-time coupling of experimental and numerical testing methods, in the field of marine hydrodynamics and ocean engineering. It is a subclass of the well known hardware-in-the-loop (HIL) testing, aiming at simulating and actuating secondary processes instead of modelling them physically (or even not including them) in hydrodynamic model tests. This method has been successfully applied by Sintef Ocean/NTNU (by the name ReaTHM^{TM}, as trademarked by Sintef Ocean) to the real-time actuation of wind loads on a floating wind turbine subjected to hydrodynamic loading. A research project to further develop this method is ongoing.

The development of force-controlled linear actuators based on position-controlled servomotors has been a central task in this field, and necessitates further improvements. The current solution consists of a torsion spring connected to the motor on one side and to a pulley on the other side. The latter pulling on a pretensioned wire to achieve linear force control. The force observer and controller currently implemented are exceedingly simple, and tuned mostly based on trial-and-error. Particular issues related to inaccuracies in the observer and excitation of eigenmodes must be addressed.

1.2 Objectives

The thesis presents the design of a force-actuating system, and discusses challenges related to the actuation of forces. There are two main objectives; *(i)* to provide more information on this relatively new topic in the field of ocean engineering and *(ii)* to develop a force-actuation system for use in real-time hybrid model testing. A literature review will be important to familiarize with already existing work done on the topic. The approach is then to start developing a test setup, providing information on the method as problems are identified and solutions are proposed.

1.3 Scope of work

The candidate should, together with Truls Hamland, cover the following main points

1. Present and discuss the method of real-time hybrid model testing, in the field on ocean engineering
2. Present and discuss the development of a force-actuation system to be used in real-time hybrid model testing by
   (a) Proposing a test case and design a hybrid test loop
   (b) Acquire the necessary components for force-actuation, position measurement, force measurement, etc.
3. Clarify challenges associated with the establishment of a valid test
4. Perform an experimental verification and validation of the system
   (a) Specify relevant KPIs (Key Performance Indicators), and study their sensitivity to parameter variations

Since the thesis presents a collaboration project between two candidates, some chapters will be similar to what is found in the thesis of Truls Hamland. Part I of the thesis and Chapter 7 is prepared as a joint work.

1.4 Limitations

A real-time hybrid test setup is developed from scratch, starting January 2017. Necessary components are determined, and acquired if not already available. Software and hardware was not familiar to the candidate prior to the project, and establishing communication between units took time. This has been the main limitations, as less time was spent on writing the thesis and exploring available literature. The DC-servomotor used in the development of a force-actuation system does not show satisfactory performance, as it introduces large time delays to the system. Such a limited actuator performance challenges the development of a valid system.

Part I

The concept of force-based real-time hybrid model testing

Chapter 2

Real-time hybrid model testing

Real-time hybrid model testing is a testing method that combines the efficiency of numerical simulation with the realism of experimental analysis. The term hybrid reflects the fact that a part of a structure is numerically modeled while the remainder is physically tested.

2.1 Background

To be able to understand the dynamics/behaviour of complex mechanical systems, physical testing has been - and still is - important. Sophisticated models and numerical tools have been developed to analyze such systems, but still some physical phenomena are not yet fully understood, nor modelled numerically (Chabaud, 2016). Examples are turbulent fluid flow, shock waves and impulse forces. The effect of these phenomena usually needs to be studied by physical testing, typically in model scale. However, physical testing also has limitations. For physical tests in model scale, errors due to scaling effects are of concern. In some cases it is also a problem that the actual model may be difficult to build or take long time to complete. Some properties may be hard to adapt to smaller structures, and other physical properties - like stiffness - may be impossible to recover in a model.

In many cases there now exist numerical models that accurately describe parts of the structure dynamics. Thus, it is proposed to divide complex structures into two parts: one that is modelled physically and one that is modelled numerically. The physical and numerical substructure will then interact in real-time through a network of sensors and actuators. By doing so, the advantages of numerical modelling are exploited while still capturing the most uncertain physical phenomena by physical testing. The concept of real-time coupling of experimental and numerical testing methods has the potential of enhancing convenience and reduce cost.

2.1.1 ReaTHM testing

Testing methods based on coupling of numerical and experimental methods in real time, have been used in different fields of engineering - and often under various terminology. In the field of earthquake engineering the term "real-time hybrid testing" is commonly used, while the synonym "Real-time dynamic substructuring" seems to be preferred by mechanical engineers (Chabaud, 2016). The name "model-in-the-loop" (MiL) has been used in the automotive industry to describe the same concept (Plummer, 2006).

When applying the method to the field of marine technology, the term *Real-Time Hybrid Model testing* (or ReaTHM^{TM} testing) has been suggested. The name is meant to indicate the concept of substructuring and computer simulation in *Froude scaled real-time*, while also illustrating the area of application. The use of "model testing" after "real-time hybrid" is meant to show the natural connection to classical hydrodynamic model tests.

2.2 HIL and real-time hybrid testing

Both real-time hybrid testing and hardware-in-the-loop simulation are forms of real-time simulations. They differ from conventional real-time simulation by the addition of a real component in the loop. Traditional real-time simulations consists of purely mathematical models of the system, simulated by a computer. Real-time hybrid testing and HIL, on the other hand, includes a mathematical model and one or more physical components in the loop. HIL is often used to verify a control system of a mechatronic system. Mechanical and electronic parts are included physically to emulate the real application environment, while a simulator represents the plant (or physical environment). HIL simulation is used instead of connecting the embedded system to the real plant, and the goal is to test the hardware device on a simulator before it is implemented on the real process. HIL simulation is an efficient way of testing hardware before the real plant is built, and one avoids damaging the real plant (or equipment, people, environment, etc). HIL testing is also efficient to individually test different parts of the system. For instance, when testing a controller in a HIL setup, you could detect errors and even tune the controller. The latter will of course require that the mathematical model used in the simulation is an accurate representation of the real process.

Real-time hybrid testing is a subclass of HIL. The method refers to the model of the plant, and hence to the division of the plant into a numerical part and physical part. This combines the efficiency of numerical simulation with experimental analysis. Since the numerical and physical parts are two different environments, interfaces have to be used to establish contact between them. The interfaces are only designed to exchange physical and numerical quantities between the two sub-

structures, and should not influence them at all. These interfaces may induce undesired delay and dynamics which need to be compensated for, and the challenge of real-time hybrid testing is their influence on the test results. This is a fundamental difference between classical hardware-in-the-loop and real-time hybrid testing.

2.3 Real-time hybrid model testing in ocean engineering

Physical model testing of marine structures in controlled environments is extensively used to understand and characterize the behaviour of floating structures subjected to environmental forces. There are many phenomena related to hydrodynamic loads that are not yet fully understood, and these have to be analyzed through physical testing. Examples are extreme wave loads (slamming, ringing and green-water on deck), viscous forces and wave-body interaction effects. It is clear that physical model testing must be done to capture the most complex and uncertain hydrodynamic forces subjecting the structure. Yet, physical model testing also has its limitations and difficulties.

Due to scaling effects, simultaneous modelling of both aerodynamic and hydrodynamic loads are challenging to obtain. The scaling of hydrodynamic model tests must be done according to the Froude number (describing the ratio between inertia forces and gravitational forces). However, in order to model the aerodynamic loads correctly, the Reynolds number (ratio between inertia and viscous forces) should be the same in model and full scale. Both numbers cannot be maintained simultaneously, and an error in the aerodynamic loads occur when scaled according to the Froude number. The result is a large increase in viscous drag forces.

In some cases, limitations in size of the test facility can be a problem. To model the mooring of structures at deeper waters, one would need a wave basin of great depth. Existing basins are too shallow to physically model the mooring lines correctly. Because of extremely high costs of building new test facilities, it would be desirable to find a way to circumvent the problem of limitations in infrastructure.

The use of real-time hybrid model testing could solve some of the problems mentioned above. Forces that are not properly modelled physically, can be replaced by actuators applying the loads. Calculations of the forces are done online through numerical simulations of a structure part. The computed forces are then sent as inputs to the actuators, which applies the loads on the physical structure in real time. The method of real-time hybrid model testing has been successfully applied by Sintef Ocean and NTNU to the real-time actuation of wind loads on a floating wind turbine subjected to hydrodynamic loading. A research project to further develop the method is ongoing.

Chapter 3

Substructuring and actuation of numerical forces

3.1 Substructuring

A system that is subject to real-time hybrid model testing, is referred to as an emulated system. The word "emulation" is used to illustrate that the hybrid test is an imitation of a system that in reality is fully numerical.

The first thing to consider when setting up a real-time hybrid model test is the substructural partitioning of the emulated system. One must choose which components of the system to include in the physical part and which components to include in the numerical part. How the emulated system is partitioned is of course problem dependent, but in general the forces that are difficult to model physically are included in the numerical model. These forces are computed online through simulations of the numerical substructure, and applied onto the physical structure using actuators. How the effect of the numerical forces should be introduced to the physical substructure should be considered. Realization of the forces can either be motion-based or force-based. The fundamental difference between motion-based and force-based real-time hybrid model testing will be addressed in Section 3.2.

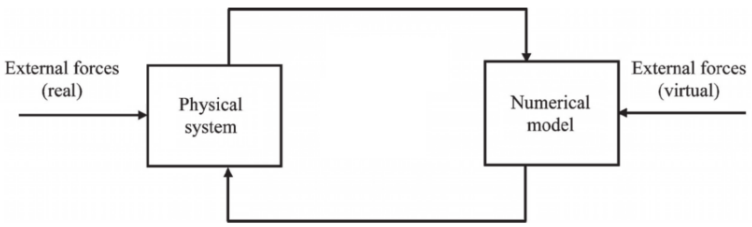

Figure 3.1: Substructuring in real-time hybrid model testing (Plummer, 2006)

Figure 3.1 illustrates the interaction between the two substructures in a real-time hybrid test. The

numerical substructure (that contains the numerically modelled part of the structure) is subjected to external forces that are virtually applied, while the physical substructure is exposed to real external forces (e.g. waves in a wave basin). Since it is the coupled response of these two system parts that is tested, they should interact.

3.2 Actuation of numerical forces

When establishing a real-time hybrid test, one is faced with the problem of how the physical model and the numerical model should interact with each other. As mentioned, the action of the numerical substructure response on the physical substructure may be either force-based or motion-based.

3.2.1 Mass-spring-damper system

To illustrate the fundamental difference between motion-based and force-based real-time hybrid testing, a simple 1-DOF linear mass-spring-damper system (see Figure 3.2a) will be considered.

$$m\ddot{x} + b\dot{x} + kx = F_{ext} \tag{3.1}$$

In the equation above, m is the mass, b is damping coefficient and k is the restoring coefficient of the mass-spring-damper system. The system is divided into a physical part and a numerical part, which together emulates the system of Equation (3.1). The numerical part of the system could include mass, damping, restoring and external forces, or just some of these forces. What to include is - as mentioned - problem dependent. In the equations below, the subscript P refers to the physical part, and the subscript N refers to the numerical part.

$$m = m_P + m_N \tag{3.2a}$$

$$k = k_P + k_N \tag{3.2b}$$

$$b = b_P + b_N \tag{3.2c}$$

$$F_{ext} = F_{ext,P} + F_{ext,N} \tag{3.2d}$$

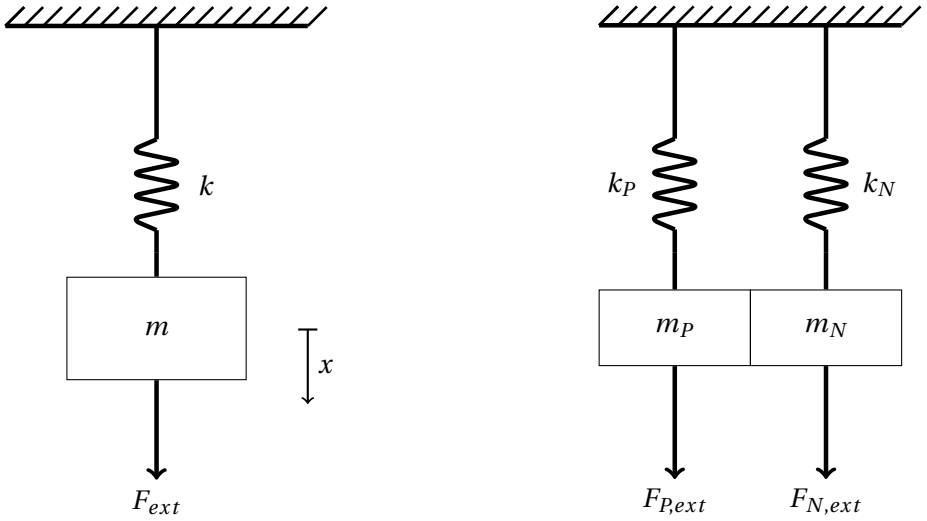

(a) Mass-spring system

(b) Substructured system

Figure 3.2: Substructuring

Looking at the two subsystem dynamics separately, Newton´s 2. law yield:

$$m_P\ddot{x}_P + b_P\dot{x}_P + k_P x_P = F_{ext,P} + F_N \tag{3.3a}$$

$$m_N\ddot{x}_N + b_N\dot{x}_N + k_N x_N = F_{ext,N} + F_P \tag{3.3b}$$

where F_N is the force induced by the numerical part of the structure onto the physical part, and F_P is the force induced by the physical part onto the numerical part. By Newton's 3. law we have the relation

$$F_P = -F_N$$

Equation (3.3a) and (3.3b) provide two equations describing the dynamics of the two subsystems, with respect to three unknowns (x_P, x_N and $F_P = -F_N$). To be able to solve the set of equations, we need a kinematic relation between the two subsystems. Such a relation will depend on the interface, and could for example be that the two masses share position ($x_P = x_N = x$) or that there is a compliant element connecting the two masses ($F_P = -F_N = k_c(x_P - x_N)$). Considering an interface where the physical and numerical substructure share position (i.e. where $x = x_N = x_P$), we obtain the equation

$$\ddot{x} = \frac{1}{m_P + m_N}\left(-b_p\dot{x} - k_p x + F_{P,ext} - b_N\dot{x} - k_N x + F_{N,ext}\right) \tag{3.4}$$

which can be put on state-space form

$$\begin{bmatrix}\dot{x}_1\\ \dot{x}_2\end{bmatrix} = \begin{bmatrix}0 & 1\\ -\frac{k_P+k_N}{m_P+m_N} & -\frac{b_P+b_N}{m_P+m_N}\end{bmatrix}\begin{bmatrix}x_1\\ x_2\end{bmatrix} + \frac{1}{m_P+m_N}\begin{bmatrix}0 & 0\\ 1 & 1\end{bmatrix}\begin{bmatrix}F_{ext,P}\\ F_{ext,N}\end{bmatrix} \tag{3.5}$$

Now, the difference between force-actuation and motion-actuation lies in how we realize the emulated system dynamics described by Equation (3.5).

3.2.1.1 Motion-based actuation

In motion-based actuation we integrate equation (3.5) in time to find the displacement to actuate at time $t + \Delta t$. Using one of the simplest time-integration schemes, namely the forward Euler method, we get:

$$\begin{aligned} x_{1,k+1} &= x_{1,k} + \Delta t \dot{x}_{1,k} \\ &= x_{1,k} + x_{2,k}\Delta t \\ x_{2,k+1} &= x_{2,k} + \Delta t \dot{x}_{2,k} \\ &= x_{2,k} + \frac{\Delta t}{m_P + m_N}\left(-(k_P + k_N)x_{1,k} - (b_P + b_N)\dot{x}_{2,k} + F_{ext,P,k} + F_{ext,N,k}\right) \end{aligned}$$

Most existing real-time hybrid testing applications use this method of motion actuation (Chabaud, 2016). But there is one big disadvantage with the method, you need to measure the physical part of the force (i.e. $-k_P x - b_P \dot{x} + F_{ext,P}$). So, if unpredictable physical dynamics are the reason for testing, this would not be a good solution.

3.2.1.2 Force-based actuation

In force-based actuation we apply the numerical force onto the physical substructure at time t. The system response at time $t + \Delta t$ is then obtained by the real, physical dynamics, and the problems of uncertain modelling of these dynamics are circumvented.

The downside of force-actuation is that it is much more challenging to actuate forces than motions. Most actuators available today are designed for velocity or position control. Force actuation would require development of new force-controlled actuators or the use of already existing position-controlled actuators in a suitable way. The latter being subject for investigation in this MSc thesis.

How to include the mass of the numerical substructure, m_N, can also be a challenge. m_N is not physical, and should be included in F_N as an inertia force $m_N\ddot{x}$, if applied to the physical substructure. The inertia force has more content at high frequencies, and with acceleration measurements being exposed to noise and drifting, this kind of force can be hard to actuate (Chabaud, 2016). An alternative solution is to include the numerical mass in the physical mass. This makes actuation easier, but is often not possible due to limiting size of the testing facility.

Chapter 4

Description of test setup

This chapter presents the design of a typical force-based real-time hybrid model test setup. The author was introduced to the method by Chabaud (2016), and thus descriptions and succeeding system designs are similar to what he has presented.

4.1 System overview

Figure 4.1 shows a block diagram of a typical real-time hybrid model test loop, and illustrates the signal flow and communication between units. The different parts of the test loop will be presented in more detail.

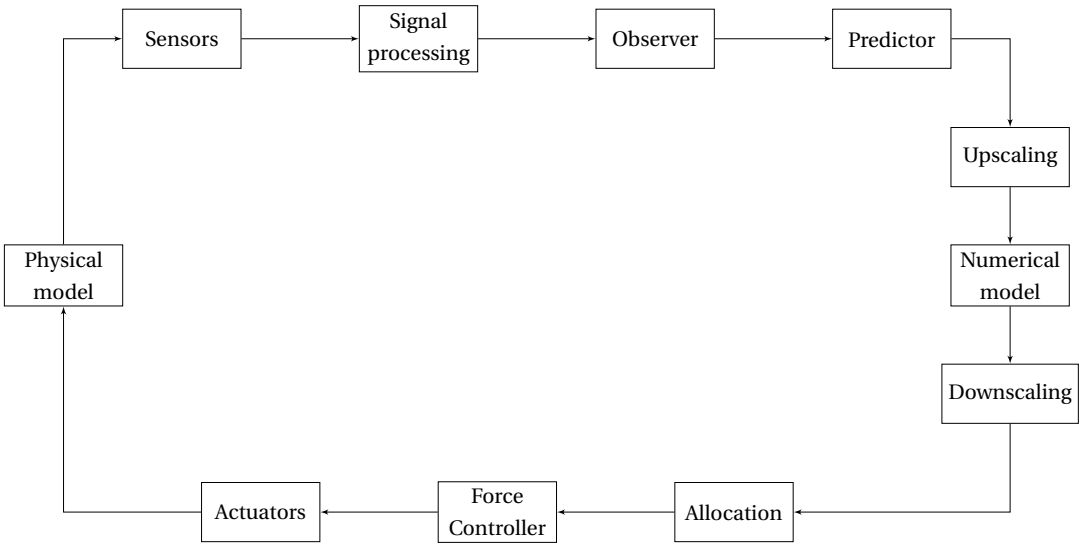

Figure 4.1: The real-time hybrid model test loop

4.1.1 Physical substructure

The physical substructure corresponds to the part of the system that is tested physically. In the field of ocean engineering, such tests are usually done on Froude scaled models.

4.1.2 Sensors and signal processing

A sensor system mounted on the physical model provides measurements of relevant states of the physical structure. Typically positions, angular velocities and linear accelerations of the physical structure are measured. These quantities will be used in simulations and calculations of the numerical substructure response.

4.1.3 Position Observer

A position observer is used to obtain good estimates of the physical model states. The observer should utilize all available sensor data to obtain robust, filtered estimates of the physical model states. The positions and velocities of the physical model are used both in the numerical substructure, to calculate the simulated forces, and in the actuators to compensate for motion of the physical structure.

4.1.4 Predictor

Due to calculation time, data processing, communication time, actuator dynamics et cetera, time delays are introduced in the system. To compensate for delays, predicted values of the physical structure motions are sent as input to the numerical substructure and the actuation system. We want to apply the calculated loads at the time the physical structure actually has reached the predicted position. By identifying the time delays and predicting with the same amount of time in the future, we ensure consistency of the physical-numerical coupling.

4.1.5 Numerical substructure

The numerical substructure represents the part of the emulated system that is modelled numerically. The response of the numerical substructure usually depends on motions of the physical substructure. Using positions and velocities of the physical model, a reaction force between the two system components is calculated online. When this force is applied to the physical substructure, the hybrid test loop is closed, and a coupled response of the two substructures is obtained.

4.1.5.1 Upscaling and downscaling

Upscaling is done because the physical system is a Froude-scaled model and the numerical simulation typically is done in full scale. Output forces of the numerical substructure must then be downscaled before applied to the physical substructure model.

4.1.6 Allocation

In an over-actuated hybrid test, one must decide which actuators to use and how large loads they should apply to the physical model. These kinds of calculations and algorithms are typically referred to as force allocations.

4.1.7 Actuators and force controllers

Based on reference forces from the allocation, controllers provide control signals which are sent as inputs to the respective force-actuators. Design and implementation of a force-actuation system and force-controller will be topic in the succeeding parts of this thesis.

Part II

Design of force-actuation system and 1-DOF real-time hybrid model test

Chapter 5

Introducing the test

The last three parts of this MSc thesis will present the design and performance of a force-actuation system and a force-based real-time hybrid test. A real-time hybrid test loop will be developed, and system tests are carried out. The motivation has been to provide more information to the field of work, more than carrying out valid tests. Less time is thus spent at testing the system emulation, and more time will be used to discuss implementation of the real-time system with use of a force-actuator.

5.1 System subjected to testing

A 1-DOF mass-spring-damper system has been subject to testing. The system consists of two connected mass-spring-damper systems, with an external force pulling the lower mass. The system is illustrated by Figure 5.1a. The choice of system can be understood from its deterministic properties and flexibility with regard to dynamics. By changing mass or spring stiffness of the system, natural frequencies are easily adjusted. Such a simple 1-DOF mass-spring-damper system actually has great similarity to many physical problems; linear modelling of mooring line forces could be an example.

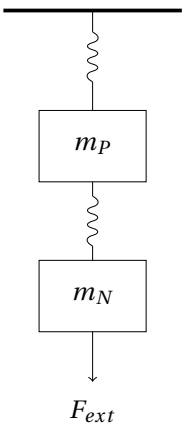

(a) System subjected to testing

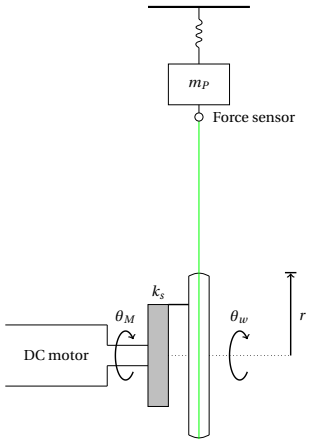

(b) Physical substructure and force-actuation system

Figure 5.1: System emulation

The lower mass-spring-damper system is considered as the numerical substructure. This numerical substructure is simulated online, and acts on the physical substructure using a force-actuation system. Figure 5.1b illustrates the real-time hybrid test emulation of system 5.1a, where the numerical substructure is replaced by a simulation and a force-actuation system. The force-actuation system will be described in more detail in Chapter 6.

5.1.1 Frequencies of interest

Before designing a real-time hybrid test, it will be important to decide which frequencies one wants to reproduce in the test. Working with a force-actuation system of a certain bandwidth, one should agree upon a limited frequency range of interest. Usually it is the dynamics of the physical substructure that is studied by tests, and the natural frequency of this physical substructure would therefore provide for the frequencies of interest. High-frequency forces will only have a small effect on slow physical substructure dynamics, and excluding these frequencies from the frequency range of interest could be considered acceptable.

Frequencies of up to 3 Hz are chosen as the frequencies of interest. The hybrid test loop will have a sampling period of 20 ms, and by the Nyquist sampling theorem this is considered to be a realizable frequency range to capture.

5.2 Numerical substructure model

The numerical substructure is connected to the physical substructure mass by its spring. The dynamics of the numerical substructure will be determined by the numerical substructure mass, spring stiffness and damping coefficient, together with positions of the physical mass and numerical mass.

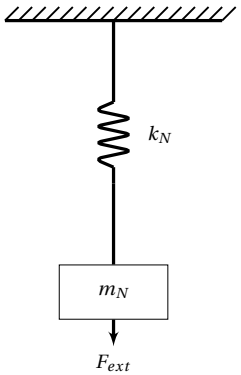

Figure 5.2: Numerical mass-spring-damper substructure

By Newton´s 2. law, the numerical substructure dynamics are given by:

$$F_{ext} + m_N g - b_N \dot{x}_N - k_N (x_N - x_P) = m_N \ddot{x}_N$$

where m_N is the numerical substructure mass, b_N is the numerical substructure damping constant and k_N is the numerical substructure spring constant. x_P is the vertical position of the physical mass, and x_N is the position of the numerical mass. F_{ext} is an external force that is virtually applied to the numerical substructure mass.

Considering the force F_N applied by the numerical substructure on the physical substructure as output, the numerical substructure state-space model becomes:

$$\begin{bmatrix} \dot{x}_N \\ \ddot{x}_N \end{bmatrix} = \begin{bmatrix} 0 & 1 \\ -\frac{k_N}{m_N} & -\frac{b_N}{m_N} \end{bmatrix} \cdot \begin{bmatrix} x_N \\ \dot{x}_N \end{bmatrix} + \begin{bmatrix} 0 & 0 & 0 \\ \frac{1}{m_N} & -\frac{k_N}{m_N} & 1 \end{bmatrix} \cdot \begin{bmatrix} F_{ext} \\ x_P \\ g \end{bmatrix} \tag{5.1}$$

$$F_N = \begin{bmatrix} k_N & 0 \end{bmatrix} \cdot \begin{bmatrix} x_N \\ \dot{x}_N \end{bmatrix} + \begin{bmatrix} 0 & -k_N & 0 \end{bmatrix} \cdot \begin{bmatrix} F_{ext} \\ x_P \\ g \end{bmatrix} \tag{5.2}$$

This numerical substructure state-space model will be used to calculate the numerical force acting on the physical substructure in a force-based real-time hybrid test.

5.3 Real-time hybrid test loop

Figure 5.3 shows a block diagram of the real-time hybrid test loop that is developed. The block diagram shows a physical substructure and a numerical substructure, interacting through a network of sensors, signal processing, mathematical calculations and a force-actuation system. The physical substructure is physically tested, while the numerical substructure is simulated online.

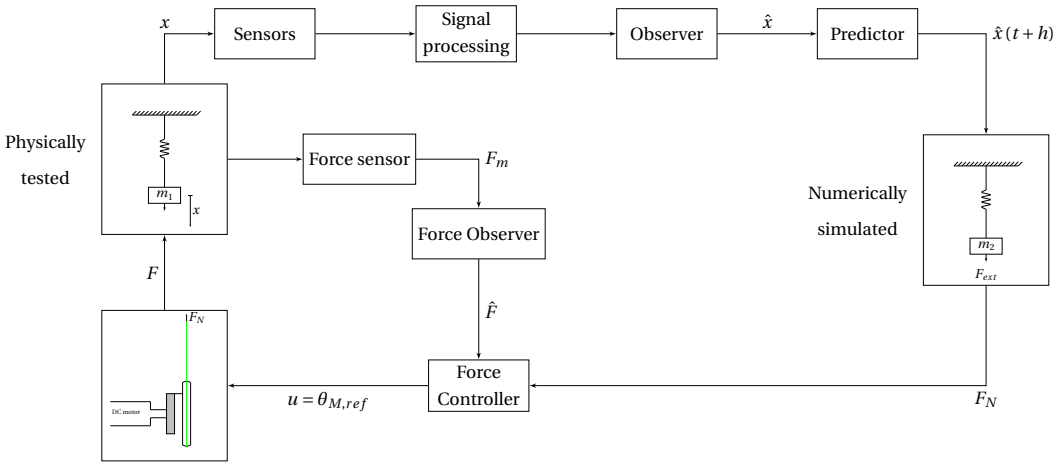

Figure 5.3: Real-time hybrid test loop

Some of the loop components should be familiar to the reader already, the others will be presented in later sections of the thesis.

Chapter 6

Force-actuation system and components

In the field of earthquake engineering, hydraulic actuators are the most common for use in real-time hybrid testing. Hydraulic actuators are usually used at high frequencies to apply deformations on the physical substructure, and hence used as motion actuation. They are capable of applying high loads, and the dynamics of such actuators are widely studied. However, the marine environment is not concerned with such seismic loading. The environmental loads on model scale offshore units are of lower order of magnitude, and as addressed earlier they should be force actuated. Electric actuators could be used, being more flexible with regard to control and operation. However, the design of such an actuator setup needs to be considered in order to obtain feasible results utilizing the real-time hybrid testing method for marine applications.

6.1 Force-actuation system

In force-based real-time hybrid model testing, one wants to apply a reference force onto a moving physical substructure. This section discusses how this could be done, and presents a setup similar to the one used by Chabaud (2016). This actuator setup will be used to apply forces of the numerical subsystem onto the physical mass-spring-damper subsystem of Chapter 5.

6.1.1 Servomotor

Both the bandwidth and the amplitude range are important properties of the actuator system. The amplitude range of the actuators should cover the amplitudes of interest, but not necessarily more. Actuators that are able to apply large forces/moments, are typically not that accurate when it comes to applying smaller forces. In real-time hybrid model testing, one is interested in environmental loads on models of floating structures. Since these loads are of small magnitude, servomotors (DC-motors with integrated control) are found suitable because of their flexibility when it comes to control and

operation.

However, these servomotors usually come with an integrated controller that provides position or speed control. Torque control is also a possibility, but since torque feedback is typically not supported, the control becomes of open-loop (Chabaud, 2016). Accurate control will then rely on correct estimates of the rotor inertia. If there is a rigid connection between the rotor and the structure, this inertia will be very difficult to measure since it depends both on the rotor itself and on the structure it is connected to. A compliant element could solve the problem, making the rotor inertia constant and easier to measure. The need for a compliant element makes torque control less attractive, and position control with force-feedback seems like a better choice.

6.1.2 Transmission

A transmission system that converts angular positions of a servomotor into forces applied on a physical model is needed. The request for a compliant element has been addressed. A transmission system similar to the one used by (Chabaud, 2016) will be described next.

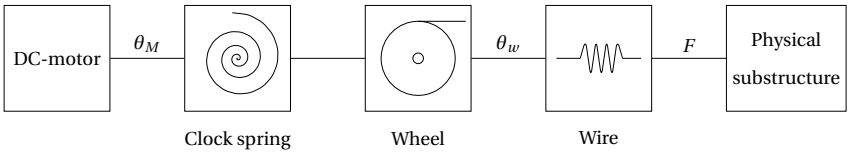

Figure 6.1: Transmission from motor angle to applied force

A clock-spring is chosen as the compliant element. The clock-spring is used as an elastic connection between the servomotor and a wheel (or pulley), which acts on the physical model through a wire. The force applied by the wire on the physical structure, can be measured and used in force-feedback control. The setup is illustrated by Figure 6.1, and depicted in Figure 6.2.

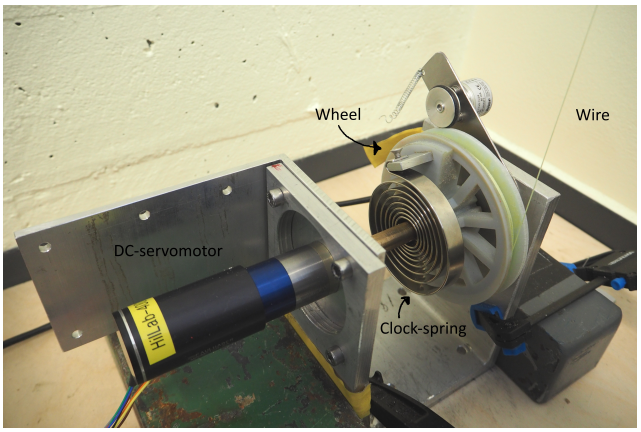

Figure 6.2: DC-servomotor and transmission system

6.1.2.1 Compliant element

The clock-spring is used as an elastic connection between the servomotor and the wheel. A clock-spring provides an almost linear stiffness. By utilizing the linear stiffness properties of the spring, we can calculate a force based on an angular displacement. We can go from position of the servomotor to a known torque applied to the clock spring.

Figure 6.3: Clock-spring (http://www.lesjoforsab.com)

The clock-spring used in this thesis is produced by Lesjöfors. The spring stiffness is calculated in Section 6.1.3.

6.1.2.2 Wheel

A wheel converts rotations of the servomotor shaft and clock-spring into linear motions of the wire. The angular position of the wheel may serve as a reference when calculating the clock-spring torque.

When designing the wheel, there is a trade-off between rigidity, inertia and radius. It is desirable to have a wheel of small inertia, so that it becomes easier to control. The request for large radius can be understood from disturbance considerations. With a large radius, the servomotor needs to adjust less to compensate for disturbances in the form of unpredictable movements of the physical substructure. The wheel that is used has a radius of 0.05 m and a mass of 0.15 kg. It is provided by Sintef Ocean, and depicted for example in Figure 6.2

6.1.2.3 Wire

The force is applied to the structure through a wire. A FireLine fishline will be used as wire. Ideally one would like a wire that has a high stiffness and a small mass, so that the effect of the wire dynamics on the applied force is as small as possible. A high stiffness and a small mass will result in a high natural frequency, which is easily filtered from the force measurements. If the mass of the wire is small, one can assume that the wire tension is constant through the wire length. By assuming a high stiffness of the wire, one can also establish a kinematic relation between the wheel angle and the physical structure position, where the two masses are considered rigidly connected. In that case, the wheel angle could be estimated from position measurements of the physical model, or the other way around.

6.1.3 Identification of spring stiffness

The torque applied to the clock-spring is determined by the linear spring constant, k_s, and an angular displacement. The angular displacement is given by the difference in angle between the motor and the wheel.

$$k_s(\theta_M - \theta_w) = Fr$$

By plotting the angular displacement against measured applied force, one can find the spring constant. Figure 6.4 show a linear regression used to find the spring constant. The plot is generated by changing the motor reference angle, θ_M, and holding the wire fixed.

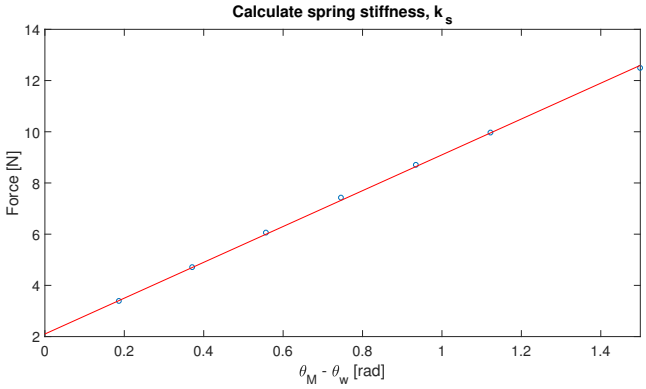

Figure 6.4: Linear regression to find the clock-spring stiffness

From the slope of the linear regression line, the spring constant is found to be:

$$k_s = 6.9974r = 0.3499 \text{ [Nm/rad]}$$

Chapter 7

Software and hardware components

7.1 Communication

7.1.1 LabVIEW

The real-time hybrid test loop is developed in LabVIEW (Laboratory Virtual Instrument Engineering Workbench) from National Instruments. LabVIEW is a system-design platform and development environment for a visual programming language, and is commonly used for data aquisition, instrument control and industrial automation. The graphical language is named "G", and is a dataflow programming language. Execution is determined by the structure of a graphical block diagram. One benefit of using LabVIEW is the extensive support for interfacing with different devices, such as motors, cameras, sensors, and displays.

7.1.2 CompactRIO

LabVIEW includes built-in support for NI hardware platforms such as CompactDAQ [1] and CompactRIO [2]. The real-time hybrid model test developed in this MSc thesis is realized with the use of a CompactRIO. The CompactRIO eliminate the need for separate subsystems by connecting components directly to the CompactRIO Controller with built-in processor I/O's, such as Gigabit Ethernet, serial ports, USB ports and C series I/O modules. National Instruments provide a wide range of C series I/O modules for different tasks, and easy access to devices through LabVIEW. The CompactRIO is shown in Figure 7.1:

[1] DAQ = Data Acquisition
[2] RIO = Reconfigurable Input Output Modules

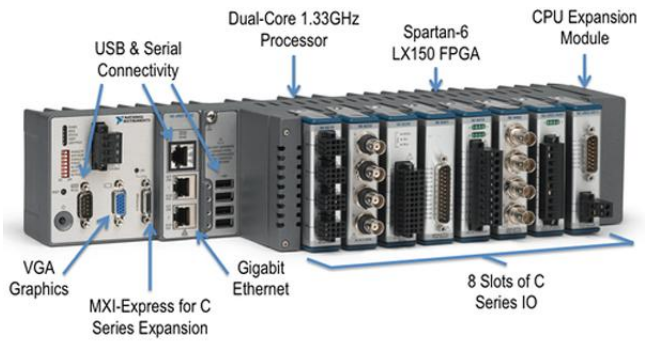

Figure 7.1: CompactRIO 9081

7.1.3 Communication between units

LabVIEW offers two possibilities when using CompactRIO:

- Scan Mode: Gives the opportunity to access each I/O module directly in LabVIEW Real-Time, and host applications with no FPGA programming. Scan Mode updates I/O variables at a user specified rate, and the maximum rate is given to be 1 kHz stated by National Instruments.
- LabVIEW FPGA: A user programmable FPGA (Field-programmable gate array) to implement high-speed control and custom timing and triggering directly in hardware. FPGA is a reprogrammable silicon chip, and gives maximum flexibility and performance[3].

LabVIEW is run in hybrid mode, meaning that both Scan Engine and FPGA are used simultaneously. The sampling period of the timed loop in LabVIEW is chosen to be 20 ms, providing enough time for necessary calculations. The reason for using hybrid mode is that communication with the encoder is programmed using FPGA (Code provided by Torgeir Wahl at NTNU). The rest of the code is programmed using Scan Engine. FPGA is faster, but requires more programming and needs to be compiled (which takes some time). For fast development of code and easy access to motor, force sensor and ultra sound position sensor, the system is run in hybrid mode. Another argument for not using FPGA exclusively, is that communication with the motor is done through the built-in serial port that is not supported by FPGA. It should be stated that an exclusive use of FPGA could result in a faster system. However, with a limited time for development of the system, the hybrid mode is chosen.

[3] http://www.ni.com/white-paper/7338/en/

7.2 Instrumentation

7.2.1 Ultrasonic position sensor

An ultrasonic range module[4] is used to measure position of the physical structure mass. The range of the ultrasound device is given to be 2cm - 4m from manufacturer. The device works best on a clean surface. The ultrasound sensor does not send signals in a straight line, but with a measuring angle of 15 degrees, see Figure 7.2a. Depending on distance to the object, the ultrasound device may pick up distance measurements from nearby objects, creating distorted signals. This is a problem since the wire and force sensor are attached at one side of the mass, and the spring to the other. In addition, the signals from the sensor contains digital measurement noise.

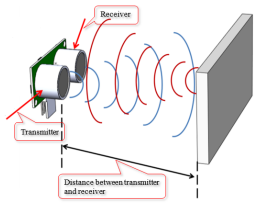

(a) Principle of ultrasound position sensor

(b) Ultrasonic Range module HC - SR04

Figure 7.2: Ultrasound position sensor

7.2.2 Encoder

To measure the angular position of the wheel, an incremental encoder from Kübler is used. The encoder has 4096 pulses per revolution. This means that the encoder can detect a change of $\frac{360^\circ}{4096} \approx 0.0879^\circ$ per pulse. The encoder is connected to - and rotates with - a small wheel with rubber surface. This small wheel is placed on top of the larger transmission wheel which was presented in Section 6.1. Figure 7.3a shows a picture of the encoder and transmission wheel assembly.

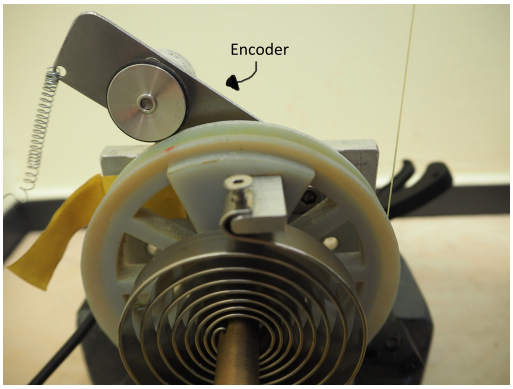

(a) Encoder and transmission wheel assembly

(b) Encoder from Kübler

Figure 7.3

[4]Name: Ultrasonic Range Module HC - SR04. Manufacturer: Elec Freaks

As the large transmission wheel (or pulley) rotates, the smaller wheel will follow its motions. If no slipping of the encoder wheel is obtained, there will be a direct relation between the encoder angle and the pulley angle. A mapping between the encoder value and the pulley angle is found by:

$$\text{Pulses per revolution of wheel} = 4096 \left[\frac{\text{pulses}}{\text{revolution}} \right] \frac{O_{wheel}}{O_{encoder}} \tag{7.1}$$

where O_{wheel} is the circumference of the pulley, and $O_{encoder}$ is the circumference of the encoder wheel.

7.2.3 Force ring

To measure the force applied by the wire on the physical substructure, a force ring is used. The force ring is provided by SINTEF Ocean and is depicted in Figure 7.4.

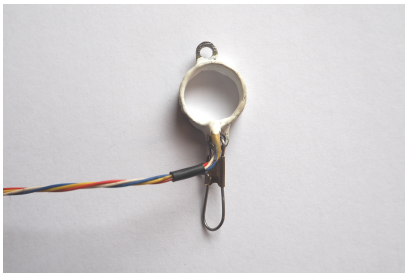

Figure 7.4: Force ring provided by SINTEF Ocean

The force ring is connected to the C-series module (NI 9237), which reads the voltage across the force sensor. The force sensor is designed so that there is a linear relation between the measured voltage, V, and the force, F, that tensions the ring. A calibration of the force ring must be done to find this linear relation. The force ring is loaded by different, known weights, and the voltage is measured. A linear fit is done to find coefficients of the line $F = aV + b$ that best fit the data points in a mean-squared sense.

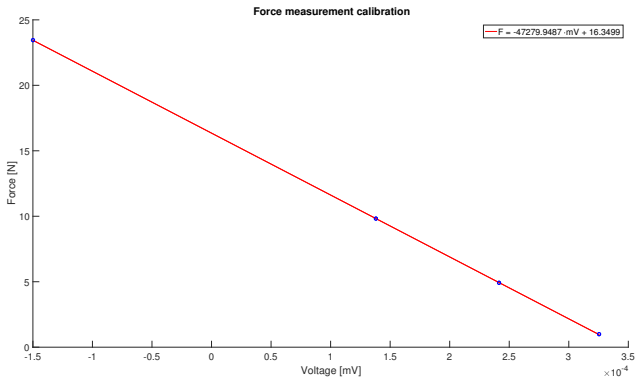

Figure 7.5: Calibration of force ring

Figure 7.5 show a linear fitting of the force ring that is used. The linear regression line is computed to be:

$$F = -47.279V + 16.350 \tag{7.2}$$

7.3 Actuator

As described in Section 6.1, a position-controlled DC-servomotor and a compliant element is used to control forces on the physical substructure. In the real-time hybrid tests, forces of amplitudes up to 20 N are considered enough. With a wheel radius of $r = 0.05m$, this corresponds to a toque of 1 Nm.

7.3.1 DC-servomotor and precision gearhead

The brushless DC-servomotor, 3564K024B, from FAULHABER was available at NTNU. Key technical data are given in Table B.1 of Appendix B. The motor is designed for a number of drive functions, including: velocity PI control, position PID control and torque control. Feedback is not supported in the torque control, and thus position control of the motor in connection with a compliant element is considered as a better choice for the relevant application.

(a) DC-servomotor (b) Precision gearhead

Figure 7.6: FAULHABER DC-servomotor and gearhead (ref. www.faulhaber.com)

The DC-servomotor provides a maximum recommended torque of 44 mNm. This would be too small for the relevant application, and a gearhead is needed to achieve motor torque of appropriate amplitude. The planetary precision gearhead, 30/1 S-43:1, from FAULHABER is chosen in order to meet the specifications. Key gearhead data are given in Table B.2 of Appendix B.

Table 7.1: Maximum available motor torque calculations

Engine maximum torque	44.0	mNm
Gearhead reduction ratio	43:1	-
Gearhead efficiency	70	%
Maximum available torque	$44 \cdot 10^{-3} \cdot 43 \cdot 0.7 = 1.3$	Nm

Table 7.1 shows the maximum torque available when using the gearhead in combination with the DC-servomotor from FAULHABER. With the gearhead in use, the motor provides a maximum force of 26 N when connected to the wheel of radius $r = 0.05$ m. This is considered enough. It should be mentioned that a gearhead will result in a slower motor, but it is needed since 44 mNm of torque would be too small.

7.3.2 Motion controller

The DC-servomotor is controlled by the FAULHABER MCBL 3006 S motion controller. The controller has numerous functions and operating modes which enable flexible adjustment to the respective drive functions of the motor. The motion controller's parameters can be individually adjusted via a PC. The "FAULHABER Motion Manager" PC software is available for commissioning and configuration of the motion controller, and can be downloaded from the FAULHABER homepage: *www.faulhaber.com*.

Figure 7.7: FAULHABER motion controller

The drive can be operated via both digital and analog inputs. To obtain a response as stable as possible, digital inputs are chosen. The RS232 interface is used for connection to CompactRIO or PC. An extensive ASCII command set is available for programming and operation. The most relevant FAULHABER motion control commands are listed in Table B.3 of Appendix B.

Chapter 8

Force-controller design

Based on the force setpoint, F_{ref}, a controller is designed to bring the system to reference by adjusting the angle of the motor. As a simplification, the DC-motor controller is assumed to work perfectly, meaning that it should provide the correct motor angle with short settling time. Later we will see that the settling time of the motor is larger than expected, and that the assumption does not really hold.

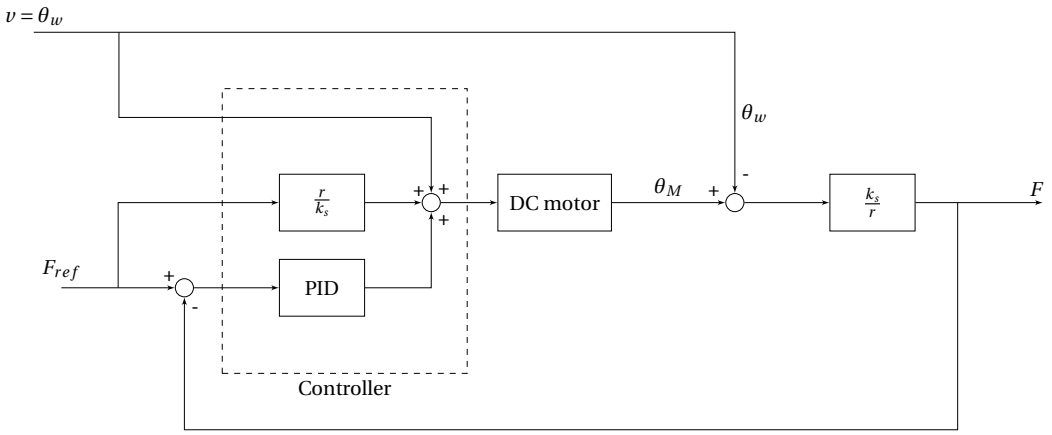

Figure 8.1: Force-control system

Figure (8.1) shows a block-diagram of the force-controller that will be used. The control action will consist of an open-loop (feedforward) control and a closed-loop (feedback) control. As the block diagram indicates, the controller has two inputs: a force reference, F_{ref}, and a disturbance, θ_w. Both the force reference and the disturbance are fed forward.

8.1 Feedforward control

A feedforward controller, based on the linear stiffness properties of the clock-spring and some system states, is developed. Figure 8.2 show the wire force acting on the wheel. k_s is the clock-spring stiffness constant, θ_M is the motor angle and θ_w is the wheel angle. By assuming a negligible mass of the wire,

one can by Newton's 2^{nd} law argue that the line tension is constant throughout the wire. If no friction is present in the system, one could estimate the force at the end of the wire, just by looking at the clock-spring torque.

In reality there will always be friction present, and in Section 11.2 it is shown that wheel friction may reduce the open-loop controller performance considerably. The dynamics of the wire will also affect distribution of the line tension, and the measured force will include some high-frequency content corresponding to natural frequencies of the wire.

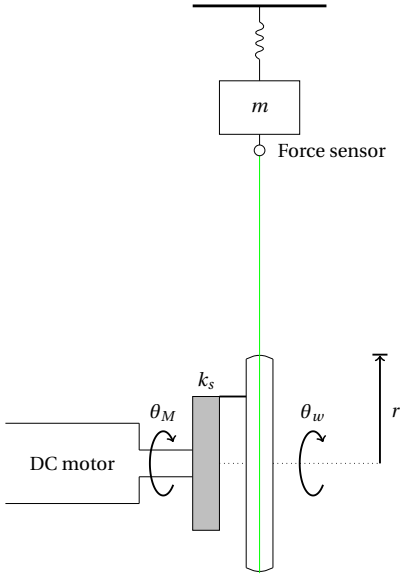

Figure 8.2: Force actuation system

The stiffness of the clock-spring provides a linear relation between the torque applied to the spring and an angular deflection determined by the motor and wheel positions.

$$k_s(\theta_M - \theta_w) = Fr \tag{8.1}$$

We are looking for an open-loop control, such that in theory:

$$\lim_{t\to\infty} F = F_{ref}$$

Where F_{ref} is the reference force we want to apply to the physical substructure. Using relation (8.1), an open-loop control is given by:

$$\theta_{M,ref} = \frac{F_{ref} r}{k_s} + \theta_w \tag{8.2}$$

Since the transmission dynamics itself is asymptotically stable, this feedforward control should bring the transmission system to reference, applying the reference force onto the physical substructure.

8.2 Feedback control

On top of the feedforward control, a feedback control is added to compensate for uncertainties in the model. The feedforward control (8.2) is based on the assumption that we know some key properties of the transmission system (i.e. in this case the clock-spring stiffness, k_s). Exact knowledge about such system properties is usually not possible to obtain, and in reality the assumption of linear stiffness does not hold exact. The feedforward control action would lead to an error between the reference force, F_{ref}, and the applied force, F. A feedback term in the control algorithm can correct for these uncertainties. For time delay problems, closing the loop could enhance accuracy by a delay compensating effect, but also lead to instability of the system. Feedback control should therefore be handled with care.

A force-output feedback PID control is considered. The PID control action is based on the error between the force setpoint and the measured/estimated output force, $e = F_{ref} - F$. The correction is calculated as the sum of three contributions: a proportional-, an integral-, and a derivative term. The feedback control signal is given by Equation (8.3).

$$\theta_{M,ref} = K_p e + K_i \int_0^t e\,dt + K_d \dot{e} \tag{8.3}$$

Desired closed-loop performance of the controller is found by tuning the three parameters: K_p, K_i and K_d.

- K_p is called the proportional gain. K_p determines how much the error itself should contribute to the control signal. In general, the proportional gain will increase the speed of the control system response. However, a too large K_p would lead to oscillations and can cause instability of the system in feedback.

- K_i is the gain of the integral term. Since the error is integrated over time, even small errors would lead to an increase in the integral action. The effect is to drive steady-state errors to zero.

- K_d is the derivative gain. The purpose of the derivative term is to react to rapid changes in the system output, F. Increasing the derivative gain would cause the control system to react more strongly to the rate of change of the error. The result would be a faster response of the overall control system. The derivative term is very sensitive to noisy signals, and thus the gain of the derivative term is often chosen to be small. For noisy feedback signals, the derivative term could cause instability of the system.

8.3 Controller performance

The purpose of the force controller is to bring the force-actuation system to reference fast and accurate. That is, the control signal should provide the necessary change in motor angle, so that the requested force is obtained at the output of the transmission system. The controller performance can be evaluated by how it reacts to changes in setpoint, F_{ref}, and disturbance θ_w.

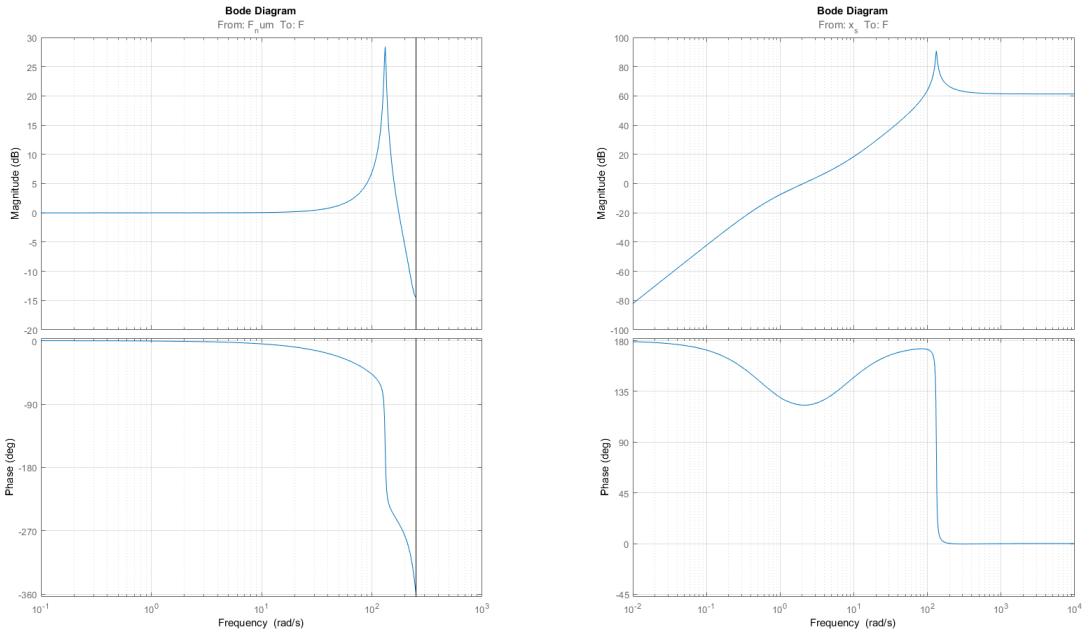

Figure 8.3: Bode plots of fully numerical model transfer functions

Figure 8.3 show examples of closed-loop Bode plots of transfer functions from force reference to applied force, and from disturbance to applied force. The transfer functions are generated from a fully numerical model of the force-actuation system, and is meant to illustrate some important properties of the force controller. In this section, the concepts of controller bandwidth, force-tracking and disturbance rejection will be presented with reference to Figure 8.3.

8.3.1 Force tracking and disturbance rejection

How well the controlled force-actuation system is able to apply reference forces on the physical substructure, is often referred to as the force-tracking capabilities of the controller. One can see that the feedforward controller developed in Section 8.1 contains two contribution. One part contributes to the mapping of reference forces, whereas the other is meant to suppress the effect of disturbances (or movements of the physical substructure). The force-tracking part of the feedforward control is given by:

$$\theta_M = \frac{F_{ref} r}{k_s}$$

The Bode plot on the left side of Figure 8.3 shows an transfer function from setpoint to applied force. One can see that for small frequencies, the force-tracking capabilities of this controller are good. The magnitude gain is 1 (or 0 dB) and the phase is 0 deg, meaning perfect mapping of the reference. For larger frequencies, the force-tracking capabilities are weakened. This is seen by a magnitude gain different from unity, and a drop in the phase.

When the physical model of Figure 8.2 moves, the controller should make the effect on the applied force as little as possible. This is called disturbance rejection. Usually the best way to compensate for disturbances, is an effective feedforward control, utilizing the measured position of the physical model or the wheel angle. The disturbance rejection part of the feedforward control is given by:

$$\theta_M = \theta_w$$

On the right side of Figure 8.3 one will see the Bode plot of a transfer function from disturbance to applied force. Suppression of a disturbance, is obtained if the transfer function has a magnitude gain as small as possible. In the Bode plot above, one can see that the disturbance rejection properties of the controller are good for small frequencies. As the frequencies gets larger, the magnitude gain gets larger, and the disturbance rejection seems to be weakened. One should keep in mind that this magnitude gain should be multiplied by the magnitude of the disturbance, to obtain the magnitude of the applied force. Often the high-frequency disturbances (vibrations) has much smaller magnitude than the low-frequency motions of a structure.

8.3.2 Controller bandwidth

The bandwidth frequency is defined as the frequency at which the closed-loop response magnitude is -3 dB. For frequencies up to this bandwidth frequency, the closed-loop Bode plot should show magnitude gains close to 0 dB, meaning correct mapping of the reference. In a real-time hybrid test it is desirable to have a force-actuation system of bandwidth covering the frequencies of interest, so that these frequencies are reconstructed properly in the test.

Different factors will determine the force-controller bandwidth. Sampling time of the LabVIEW timed loop and the servomotor bandwidth are important factors. The Nyquist sampling theorem states that the minimum sampling rate needed to preserve all the information in a continuous bandlimited signal, will be two times the highest frequency of the signal. If the sampling rate is less than the Nyquist rate, some information will be lost, and the original signal cannot be exactly reconstructed on the basis of the sequence of signals (Robert Grover Brown, 2012). The same theorem holds for discrete control systems, and as a "rule of thumb" the sampling frequency should be 10 times that of the fastest process one wants to reconstruct. With a sampling period of 20 ms in LabVIEW, this

corresponds to a frequency of 5 Hz.

Part III

Adapting to real-world challenges

Chapter 9

Time delays

Time-delay linear systems are well studied problems in control engineering. The introduction of a time delay into the real-time hybrid model test setup will challenge both the stability and the accuracy of a test. This chapter will discuss time-delay linear systems. Identification of time delays in the real-time hybrid test will be done, and a compensation method will be proposed.

9.1 Basic theory about delays

Time delays are always present in a real-time system, but the type of delay and its size is problem dependent. Time delays can be divided into two groups: pure time delays h and phase delays ϕ. The former group are frequency-independent delays, that may vary in time. Pure time delays typically arise from dead times in computation, communication and synchronization. Phase delays on the other hand, are delays that vary with frequency, and typically arise in inertia systems. Traditionally it has not been distinguished between pure time delays and phase delays, they have been lumped together and treated as one constant time delay (Carrion and Spencer, 2007). As described by Chabaud (2016), a total equivalent time delay can be calculated as

$$h_{eq}(t,\omega) = \frac{\phi(\omega)}{\omega} + h(t) \tag{9.1}$$

And equivalently, a total phase delay is given by

$$\phi_{eq}(t,\omega) = \phi(\omega) + \omega h(t) \tag{9.2}$$

9.1.1 Modelling and linear approximations of time delays

In the Laplace domain, the effect of a time delay h is given by an exponential function e^{-sh}. According to Kreyszig (2011), the Laplace transform of a time-shifted function f would be:

$$\mathscr{L}(f(t-h)u(t-h)) = e^{-sh}\mathscr{L}(f(t)) \tag{9.3}$$

When analyzing the effect of a time delay on linear systems, it is desirable to find a linear representation of the time delay. Several linear representations exist, and among them the so-called Padé approximation based on Taylor expansions. In its simplest form, a first order Padé approximation is given by the ratio of two first order polynomials (Jens G. Balchen, 2003).

$$e^{-hs} = \frac{e^{-\frac{h}{2}s}}{e^{+\frac{h}{2}s}} \cong \frac{1-\frac{h}{2}s}{1+\frac{h}{2}s} \tag{9.4}$$

The accuracy of the approximation is best for small frequencies. As the frequency gets larger, the Padé approximation will diverge from the true representation. So, even though Padé approximations are found suitable for the study of errors induced by relatively small delays, they may fail to study stability issues (where the phase is typically larger than 180 degrees).

The effect of a time delay on a linear system is best represented in the frequency domain. Therefore, the effective delay on a system will be the total phase delay, frequency-dependent but constant in time. In the frequency domain, a time delay is described by a magnitude gain of unity and a phase shift of ωh [rad].

$$\left|e^{-j\omega h}\right| = 1, \qquad \angle\left(e^{-j\omega h}\right) = -\omega h$$

Processes which include time delays are non-minimum phase processes. Such processes are more difficult to control because of the larger negative phase lag (Jens G. Balchen, 2003), and the control system typically needs to be slower to avoid instability. A phase diagram of three different time delays is given in Figure 9.1.

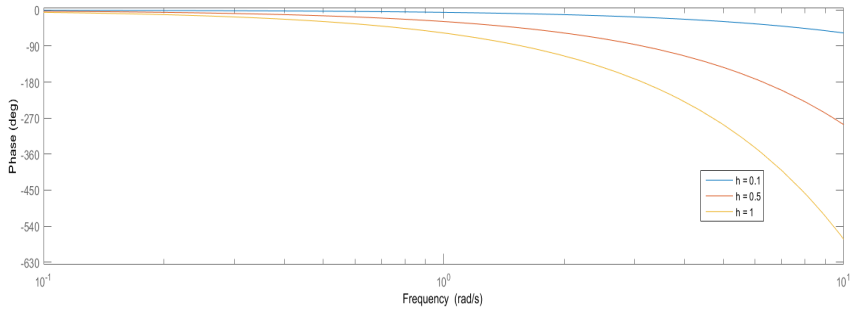

Figure 9.1: Phase diagram of different time delays.

Figure 9.1 shows that the phase lag of a linear system passing through a time delay starts at zero for small frequencies and decreases rapidly with increasing frequency, ω. Larger time delays will result in larger negative phase lags.

9.1.2 Stability of time-delay linear systems

When studying the stability of dynamic systems, it is often convenient to do it in two steps. First the stability of the open-loop system is analyzed, and then the closed-loop stability is considered. It is well known that time delays may induce instabilities to a closed-loop system. When the phase delay exceeds a critical limit, feedback creates negative damping to the system. If the magnitude of the negative damping exceeds the open-loop positive damping, it will cause the system to diverge and get unstable (Chabaud, 2016).

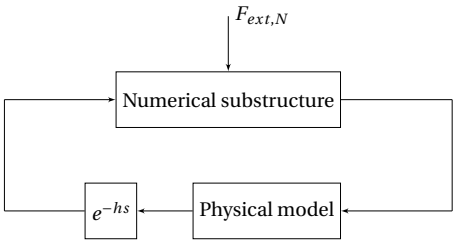

Figure 9.2: Closed-loop representation of real-time hybrid test

A real-time hybrid test is in fact a closed-loop system. The simulated loads of the numerical substructure is actuated onto the physical substructure, whose response is measured and given back as input to the numerical substructure. It is obvious that stability of time-delayed closed-loop systems will be an important topic for the test designer.

Open-loop stability

An open-loop system, $H(s)$, can be represented by the block diagram of Figure 9.3.

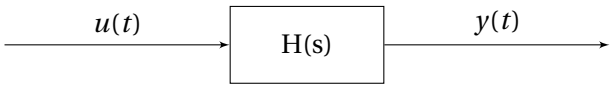

Figure 9.3: Block diagram of an open-loop system

The dynamics of a linear system $H(s)$, is typically put on state-space form in the time domain.

$$\dot{\mathbf{x}}(t) = \mathbf{A}\mathbf{x}(t) + \mathbf{B}\mathbf{u}(t)$$

$$\mathbf{y}(t) = \mathbf{C}\mathbf{x}(t) + \mathbf{D}\mathbf{u}(t)$$

Open-loop stability of a linear system, is expressed in terms of *internal stability* and *BIBO stability*. While BIBO stability is defined for zero-state responses, internal stability is defined for zero-input responses. A system is said to be BIBO stable (bounded-input bounded output stable) if every bounded input excites a bounded output. Chen (2014) gives the following definition for internal stability:

Definition 1 The response of $\dot{\mathbf{x}}(t) = \mathbf{A}\mathbf{x}(t)$ is *marginally stable* or *stable in the sense of Lyapunov* if every finite initial state $\mathbf{x}_0$ excites a bounded response. It is *asymptothically stable* if every finite initial state excites a bounded response which, in addition, approaches zero as $t \to \infty$.

Chen (2014) states that asympthotically stable systems also are BIBO stable. Note that the above definition is valid for linear systems only, and a time delay system is strictly speaking not linear. For small delays the linear approximation of time delays is considered good enough, and one assumes that the above definition holds. The stability properties of linear systems are determined by the system poles. The following theorem is given in Chen (2014):

Theorem 1

- The equation $\dot{\mathbf{x}}(t) = \mathbf{A}\mathbf{x}(t)$ is *marginally stable* if and only if all eigenvalues of $\mathbf{A}$ have zero or negative real parts and those with zero real part are simple roots of the minimal polynomial of $\mathbf{A}$.
- The equation $\dot{\mathbf{x}}(t) = \mathbf{A}\mathbf{x}(t)$ is *asymptotically stable* if and only if all eigenvalues of $\mathbf{A}$ have negative real parts.

It is worth mentioning that other than oscillators, every physical system is designed to be asymptotically stable or BIBO stable (Chen, 2014).

Closed-loop stability

Let us consider the closed-loop system of Figure 9.4. It is assumed that the system $H(s)$ is open-loop stable. Since BIBO-stability of the system $H(s)$ is provided, we know that also the closed-loop system will be stable as long as the input $u - e^{-hs}y(t)$ does not grow unbounded.

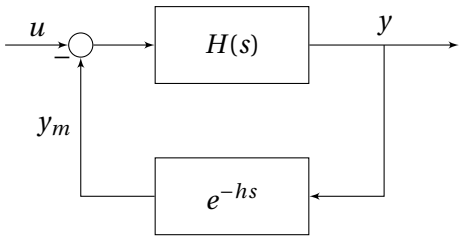

Figure 9.4: Block diagram of system with feedback delay

Closed-loop stability is easiest analyzed in the frequency domain. We break the loop at y_m, and study the response of the feedback signal without allowing it to contribute to excitation. After transient responses are damped out, the output of a linear system $H(s)$ will oscillate with the same frequency

as the input, probably with a phase shift $\phi = \angle H(j\omega)$ and a magnitude gain $|H(j\omega)|$ (Jens G. Balchen, 2003).

$$y_m(t) = |H(j\omega)| sin(\omega t + \phi) \tag{9.5}$$

As pointed out earlier, the effect of a time delay will be an increase in the phase shift of $\phi = -\omega h$. Now, if ϕ exceed the limit of -180 degrees, the feedback signal will change sign, and y_m will be added to the input instead of being subtracted. This can be seen as an introduction of negative damping to the system. If the magnitude of this negative damping gets larger than the positive open-loop damping, it will lead to instability of the closed-loop system(Chabaud, 2016).

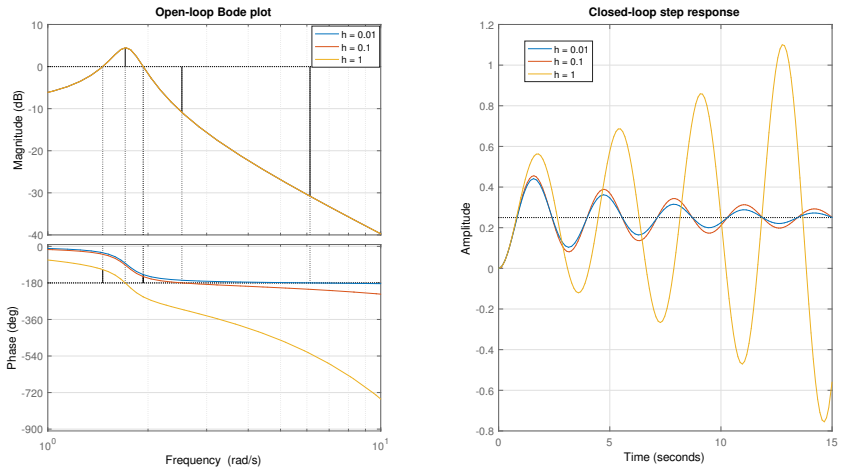

Figure 9.5: Bode plot and step response of time-delay mass-spring-damper system

Figure 9.5 show the open-loop Bode plot and the closed-loop step response of a second order system $H(s)$ with a time delay, h, in the feedback signal. Stability of the closed-loop system is assured as long as the crossover frequency ω_c is smaller than ω_{180}. As can be seen, time delays leads to a left-shift of ω_{180}, and loss of stability for large delays.

9.2 Identification

9.2.1 Sources of time delay

Time delays in real-time hybrid testing are inevitable, and may originate from different sources. The delays can be grouped into three categories: communication delays, computation delays and actuator delays.

Communication delay

Hybrid testing is a closed-loop setup, and there is continuous exchange of information between components. Information needs to travel from one node to another, and even though the transportation time is short, it does take time. A small delay is related to transfer of data, but the main communication delay comes from a sampling period in the LabVIEW code. The real-time test is programmed in a timed loop that is executed with a sampling period of 20 ms in LabVIEW. This means that samples of measured signals are collected every 20 ms, and that the motor position is adjusted in discrete steps of the same period in average. The result is a sampling delay of half the sampling period in average (Jens G. Balchen, 2003). With a sampling period of 20 ms, a time delay of 10 ms is expected.

Computation delay

A computer is used to solve equations (e.g. in the force controller and observer). The time required to do the calculations will introduce a delay in the system. The more demanding the calculations are, the more delay will be present. A faster processor or a more effective code could reduce the computation delay.

By comparing timestamps of measured inputs and calculated outputs in LabVIEW, a computation delay between measurements and control signals are found to be approximately 4 ms in the developed real-time hybrid test loop.

Actuator delay

The use of a DC-servomotor introduce additional delay to the system. Figure 9.6 show a unity step response of the motor control.

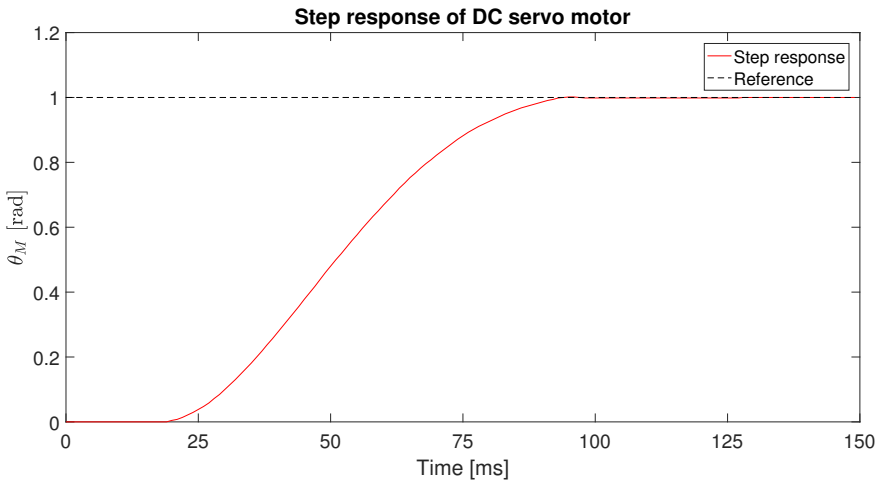

Figure 9.6: DC-servomotor step response

When the motor motion controller is asked to provide a step of $\theta_M = 1$ rad, one can see that there is a

pure time delay of as much as 19 ms before anything happens. This pure time delay is assumed to be due to communication and computation in the motion controller. In addition to the pure time delay, there is a phase delay related to the dynamics of the motor. When the motor angle start to adjust, it takes some time before it is settled at the commanded position of 1 rad.

9.2.1.1 Estimation of total delay

To summarize, there will be different sources of time delays in the real-time hybrid test setup and force-actuation system. The main delay comes from the FAULHABER DC-servomotor, which introduce a pure time delay of approximately 20 ms in addition to a frequency-dependent phase delay. The sampling time in LabVIEW will be the second major source of delay, leading to a sampling delay of $\frac{T}{2} = 10$ in average. With approximately 4 ms of computation delay, one should expect a total pure time delay of 35 ms in the system.

9.3 Compensation

As we have seen earlier, time delays challenge the stability of closed-loop systems and decrease the controller accuracy. But if magnitudes of the time delays are identified, it may be possible to compensate for them. In this section, a compensation method that predicts a system state ahead in time is presented.

As mentioned, it is distinguished between pure time delays that are independent of frequency and phase delays that may vary with frequency. Normally these delays are lumped together, and treated as a constant time delay when predicting. This means that the prediction would be most valid in a limited frequency range.

9.3.1 Polynomial extrapolation

Prediction based on polynomial extrapolations, are of the simplest, but yet most useful compensation methods. Polynomials can be used to approximate any physical process, and do not depend on a mathematical model of the system. Given a set of measurements on a time interval, one finds a polynomial of a certain degree that best fits the measurements. Different methods exists to obtain such polynomials, among them are the famous Lagrange method and Newton's divided difference method (Kreyszig, 2011). A method based on minimizing a mean-squared error will be described here. This method allows us to use a larger number of samples to build the polynomial, and thus also has a filtering effect which makes it more robust to noise in measured signals. According to Chabaud (2016), noisy signals would make polynomial extrapolation challenging.

Looking for an interpolation polynomial of degree n,

$$p_n(t) = \sum_{j=0}^{n} a_j t^j$$

we want to minimize the mean squared error (MSE) of the interpolation function at m sampling points.

$$L = \sum_{i=1}^{m} \left(p_n(t_i) - y_i\right)^2$$

This is the same as finding the zero crossing of

$$\frac{\partial L}{\partial a_i} = 0$$

For a third order polynom, this equals finding solution to the set of equations:

$$\begin{aligned}
\sum_{i=1}^{m} \left(p_3(t_i, \mathbf{a}) - y_i\right) &= 0 \\
\sum_{i=1}^{m} \left(p_3(t_i, \mathbf{a}) - y_i\right) t_i &= 0 \\
\sum_{i=1}^{m} \left(p_3(t_i, \mathbf{a}) - y_i\right) t_i^2 &= 0 \\
\sum_{i=1}^{m} \left(p_3(t_i, \mathbf{a}) - y_i\right) t_i^3 &= 0
\end{aligned}$$

which can be put on matrix form

$$\begin{bmatrix} m & \sum t_i & \sum t_i^2 & \sum t_i^3 \\ \sum t_i & \sum t_i^2 & \sum t_i^3 & \sum t_i^4 \\ \sum t_i^2 & \sum t_i^3 & \sum t_i^4 & \sum t_i^5 \\ \sum t_i^3 & \sum t_i^4 & \sum t_i^5 & \sum t_i^6 \end{bmatrix} \cdot \begin{bmatrix} a_0 \\ a_1 \\ a_2 \\ a_3 \end{bmatrix} = \begin{bmatrix} \sum y_i \\ \sum t_i y_i \\ \sum t_i^2 y_i \\ \sum t_i^3 y_i \end{bmatrix} \tag{9.6}$$

Solving the set of equations in (9.6), one finds the coefficients of a third order polynomial that best fits the measurements in a mean-squared sense. Higher order polynomials are also easily obtained, and the structure of Equation (9.6) would then be similar. Note that if the sampling time is constant, one could interpolate over a constant time interval, and then shift the function on the t-axis. By doing so, one would avoid difficulties with the matrix in Equation (9.6) growing large.

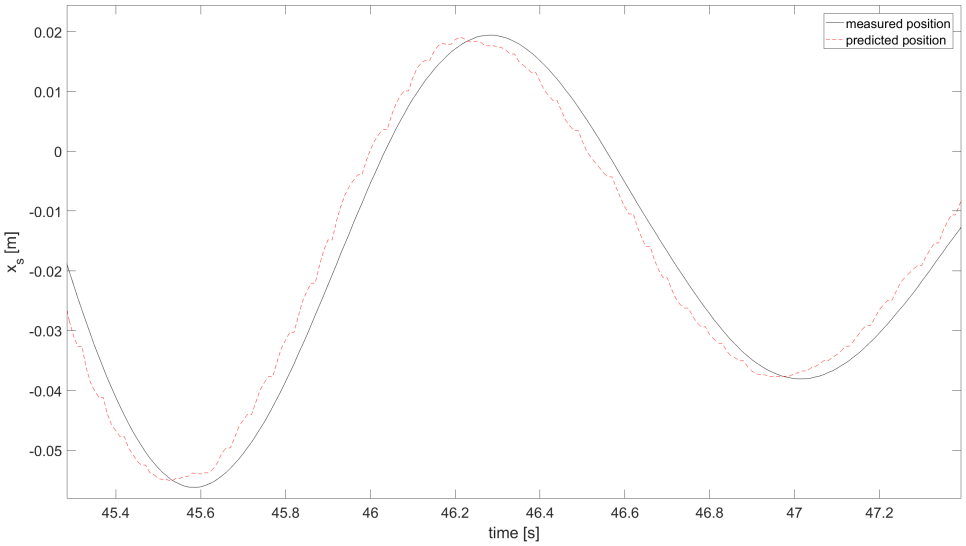

Figure 9.7: Polynomial prediction of position

Figure 9.7 shows a third order polynomial prediction of position during a decay test in following mode. The position is predicted 0.045 s ahead in time, and is based on 30 measurement samples. The figure show a predicted signal that is shifted forward in time compared to its input signal. Due to a relatively long extrapolation time, one can see a less smooth prediction signal. In succeeding sections it is seen that fluctuations of a control input could excite high-frequency eigenmodes of an elastic system. How to choose the prediction time and number of measurement samples must be considered. Generally the prediction time will depend on the magnitude of time delays, and the number of samples on the signal frequency and amount of noise in input signals. Prediction of noisy signals usually needs more samples to improve the filtering effect. Analysis of the prediction function is done in Chapter 12 of the thesis.

Both third and fifth order polynomials have been considered. The order of the polynomial should be an odd number, since its shape around origin should be similar to that of a sine wave (Chabaud, 2016). Tests show best stability properties of third order polynomials, and thus third order polynomials have been used in succeeding testing and analysis. Even though fifth order polynomials in theory have better accuracy in the interpolation interval, this might not be the case when extrapolating. Because of its fifth order term, the fifth order polynomial could "escape" the real process more rapidly outside the interpolation interval.

9.4 Time-delay induced damping

In the real-time hybrid model test, forces are applied on a physical structure by use of an elastic transmission system. Figure 9.8 show an illustration of the setup.

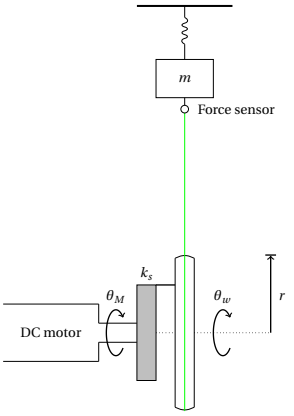

Figure 9.8: Force actuation on mass-spring-damper system

Positions of the motor and physical structure (or wheel), will together with the clock-spring stiffness, determine the force at the end of the wire. Let us consider a constant reference force given as input to the force controller. Measured positions of the wheel angle, θ_w, will be used by the controller to compensate for motions of the physical substructure. If a time delay is present in the system, the result will be a spring force due to stiffness of the transmission. This spring force will be determined by the time delay and the clock-spring stiffness. Assuming that the force-tracking part of the controller is able to provide the reference force $F_{ref} = F_0$, the force applied to the physical substructure will be:

$$\begin{aligned} F_N &= F_0 + \frac{k_s}{r}\left(\theta_w(t) - \theta_w(t-h)\right) \\ &= F_0 + \frac{k_s}{r^2}\left(x(t) - x(t-h)\right) \end{aligned}$$

where the relation $\theta_w = \frac{x}{r}$ has been used. The equation describing the physical structure dynamics becomes:

$$\ddot{x} + 2\zeta_P\omega_0\dot{x} + \omega_0^2 x = -\frac{F_0}{m_P} - \frac{k_s}{r^2 m_P}\left(x(t) - x(t-h)\right) \tag{9.7}$$

where m_P is the physical structure mass, ζ_P is the damping ratio and ω_0 is the natural frequency. Since the time delay usually is of small magnitude, the effect of the delay can be seen as an added damping to the system. The damping coefficient will be $\frac{k_s h}{r^2}$.

$$\lim_{h\to 0}\frac{k_s}{r^2}\left(x(t) - x(t-h)\right) = \frac{k_s}{r^2}\lim_{h\to 0} h\frac{x(t) - x(t-h)}{h} = \frac{k_s}{r^2}h\dot{x}(t)$$

Equation (9.7) is a so-called delay-differential equation (DDE). By comparing simulations of initial

value DDE problems with real measurements, e.g. from a decay test in following mode, DDEs can be used to estimate time delays in a system. Due to an overdamped response, this kind of delay identification did now show good results in our case.

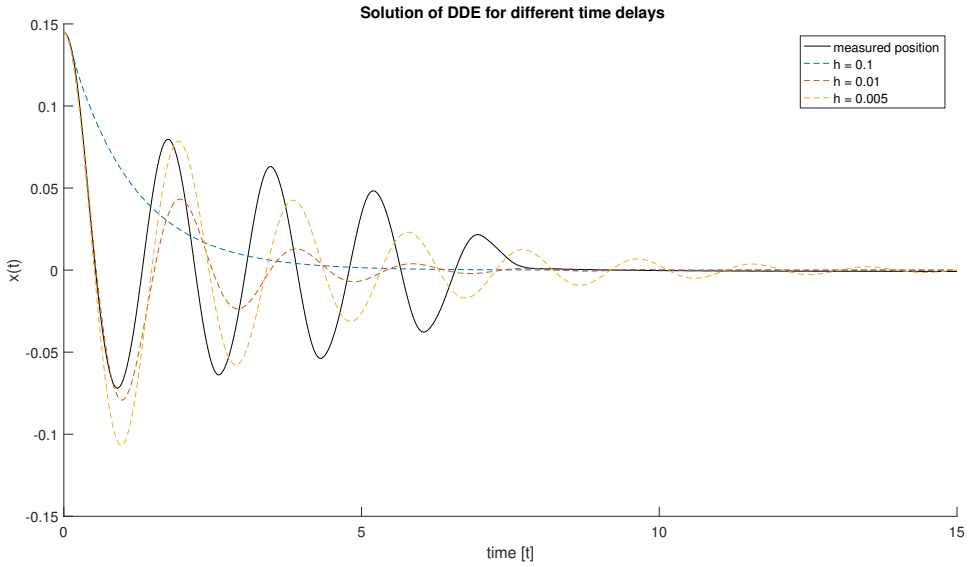

Figure 9.9: Measured and simulated response of DDE in following mode

The plots of Figure 9.9 is meant to illustrate the use of DDE solvers to estimate time delay. The plots also show the added damping induced by time delays in the system. A decay test of the time-delayed system is done in following mode. To obtain the measured response with a few oscillations, a prediction of the wheel angle 0.04 seconds ahead in time was done. The measured response is plotted against DDE simulations with different time delays. The *dde23* solver in Matlab was used to generate the simulations. The plot indicate that a delay of $h = 0.005$ is not far from what is true (when predicting). Adding this to the prediction extrapolation time, a total time delay of about 0.045 s should be expected in the system.

Chapter 10

Noise

Noise will always be present in a real-time hybrid model test. By noise we mean pollution of a signal, that may reduce accuracy and stability of a control system. In this chapter different sources of noise in the real-time hybrid test of a mass-spring-damper system will be discussed. An observer that filter noisy force measurements will be proposed.

10.1 Theory

Some basic theory about noise is presented. The theory provide basic ideas and definitions used in the succeeding discussions.

10.1.1 Measurement and process noise

Noise can be divided into two groups: measurement noise and process noise.

$$\begin{aligned} \dot{\mathbf{x}} &= \mathbf{A}\mathbf{x} + \mathbf{B}\mathbf{u} + \mathbf{G}\mathbf{w} \\ \mathbf{y} &= \mathbf{C}\mathbf{x} + \mathbf{H}\mathbf{v} \end{aligned} \tag{10.1}$$

The measurement noise $\mathbf{v}$ and the process noise $\mathbf{w}$ of a linear system, can be included in the state-space representation as Equation (10.1). Process noise relates to fluctuations between the actual state space and the modelled state space, while measurement noise relates to fluctuations between the measurement model and the true measurements. In the succeeding discussions, high-frequency vibrations and eigenmodes will be referred to as process noise.

10.1.2 Natural frequency and vibration

The natural frequency of a system corresponds to the frequency at which it oscillates in absence of a driving force. If forces are applied on a system close to its natural frequency, the amplitudes of

oscillation may become large and increase over time. The effect is seen by a peak in the magnitude Bode plot of a linear system in Figure 10.2. The phenomenon is called resonance, and is a well studied topic in the field of control engineering.

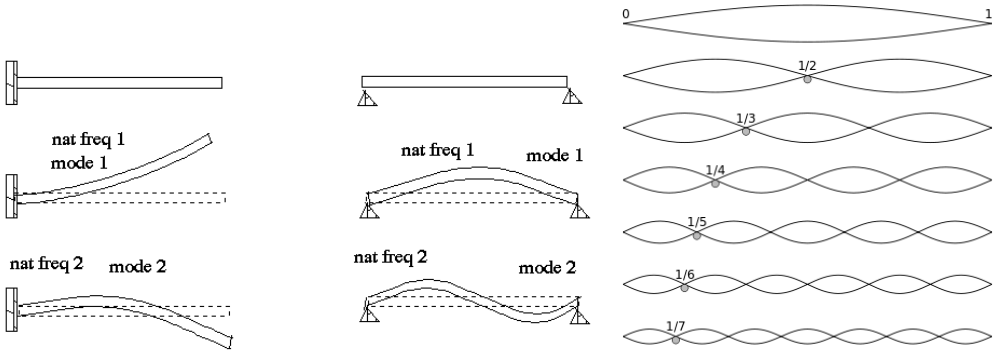

(a) Elastic beam (b) Vibrating string

Figure 10.1: Mode shapes of elastic structures

An eigenmode is a natural vibration of an elastic structure, such that various parts all move together at the same frequency. An elastic structure will typically have discrete modal frequencies and associated mode shapes. Examples of eigenmodes are shownin Figure 10.1a for an elastic beam, and in Figure 10.1b for a vibrating string. Each of the eigenmodes will have a corresponding natural frequency. The modes of lowest frequency are called fundamental modes. The other, harmonic modes will oscillate with integer multiples of the fundamental frequency.

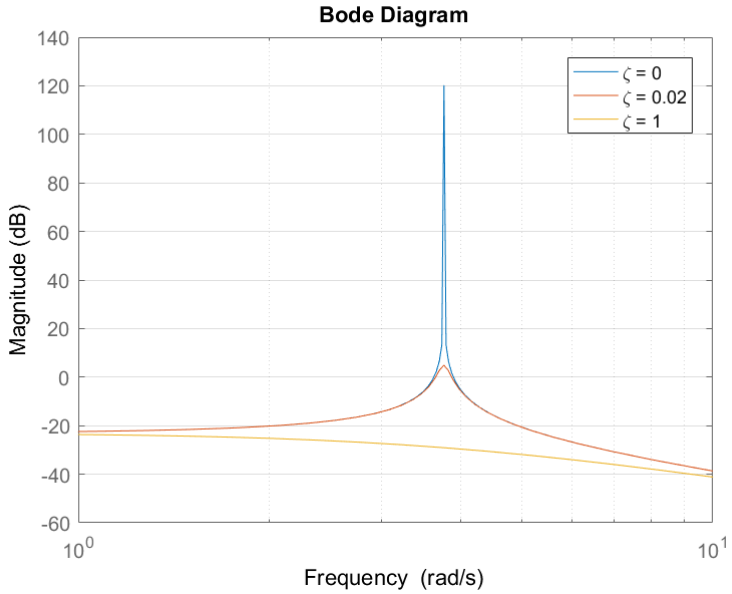

Figure 10.2: The effect of damping at resonance

As Figure 10.2 illustrates, the damping of a system will limit the response amplitudes at resonance. The figure shows the magnitude bode plot of a second order system (from input to output) subjected

to an exciting force. One can see that the damping is important for the magnitude gain at resonance. Larger damping ratio, ζ, reduce the amplitudes of oscillations at resonance.

10.2 Force control using elastic transmission system

The force controller developed in Chapter 8 utilizes the elastic properties of the transmission system presented in Chapter 6. If the controller output contains frequencies close to any natural frequency of the transmission system, these eigenmodes may be excited. The controller output has two contributions: the feedforward (open-loop) control action and the feedback (closed-loop) control. Both controls may be origin to eigenmode excitation. Their contributions to resonance vibrations will be discussed.

10.2.1 Open-loop control

Let us consider the feedforward control:

$$\theta_{M,ref} = \frac{F_{ref} r}{k_s} + \theta_w$$

The controller output, θ_{ref}, will include the same frequencies as the inputs, F_{ref} and θ_w. It is clear that high-frequency content (noise) of the measured wheel angle, will be origin to rapid fluctuations of the control signal. These rapid fluctuations of the control output, would increase wear and tear of an actuator, and could excite high-frequency eigenmodes of the system. Smooth position measurements are therefore desirable, and if the measurements are not smooth, they should be filtered. Fortunately, the encoder is very accurate and does not need to be filtered. However, predictions based on these signals are not necessary smooth (see for example Figure 9.7).

The reference force, F_{ref}, should not have content close to any natural frequency of the transmission system. Since the physical substructure usually would be of much slower dynamics compared to the transmission vibrations, these high frequencies could be excluded from the force setpoint. Their response on the physical substructure would only have a limited effect. In Section 5.1.1 the choice of frequencies of interest was mentioned.

10.2.2 Closed-loop control

The feedback control is given by:

$$\theta_M(t) = K_p e(t) + K_i \int_0^t e(\tau) d\tau + K_d \dot{e}(t)$$

where $e = F_{ref} - F$. The feedback control signal will contain the same frequencies as the inputs, F_{ref}

and F. The measured force, F, will be affected by the transmission system dynamics, and it will thus have content at the natural frequencies of the transmission. It will be shown that e.g. transverse vibrations of the wire will pollute the measured force. If the natural frequencies are fed back as inputs to the force controller, the actuator could excite these natural vibrations. To avoid amplifying the natural vibrations, it is therefore desirable to remove natural frequencies and measurement noise from the feedback signal. Filtering of the measurements could be done, but this will induce a phase lag between the measured and the filtered signal. In Section 10.5 a model-based force observer is proposed. The model-based observer provide estimates of the force with phase lags only in the unmodelled part of the estmates.

10.3 Combined force tracking and damping on elastic structures

Actuation of reference forces onto physical models is an important topic that is of concern in force-based real-time hybrid model testing. This so-called mapping of reference forces is sometimes referred to as force tracking, and may involve difficulties when applied to elastic structures.

Force-tracking in real-time hybrid model testing is achieved by use of actuators with a certain bandwidth, meaning that they are able to apply setpoint forces at a limited range of frequencies. If the setpoint of a force-controller varies with a frequency exceeding this bandwidth of the controller, the applied force would not be accurate and sometimes it may be much larger or smaller than setpoints it is meant to follow. The same argument applies to the disturbance rejection properties of a force controller. That is, the capabilities of the force-actuation system to suppress uncertain motions of the structure it is connected to and should apply forces on. Motions of the physical structure that are of low frequency - in sense of controller bandwidth - can be measured and compensated for by the controller. Usually an accurate feedforward control action, where measured positions of the physical structure is utilized, would be the best way of suppressing these disturbances. Due to limitations of the controller bandwidth, rapid disturbances are more difficult to compensate for. Therefore, one should instead of unsuccessfully try to compensate for these high-frequency disturbances, try to limit their impact on the overall actuator performance.

When tracking forces on elastic physical structures, one is faced with some of the mentioned difficulties regarding controller bandwidth and disturbance rejection. Fast and accurate tracking of forces with an aggressive controller may excite some of the flexible structure eigenmodes. Based on properties of the physical substructure, such as elasticity, cross-sectional area and length, the frequencies of the different eigenmodes may vary. Some modes could oscillate with low frequencies which controllers can compensate for, while other modes may oscillate so fast that accurate disturbance rejection is simply not possible with the actuator at hand. Instead of unsuccessfully trying to compensate

for these high-frequency vibrations, one would like to dampen them out, making their effect on the applied force as little as possible. Damping of high-frequency eigenmodes of the physical substructure is done by filtering these frequencies from the controller input signals (i.e. the measured position x or θ_w, and force F). This way one would avoid exciting these frequencies by the force-actuation system.

10.4 Flexible modes in force actuation system and physical substructure

Process noise, in form of vibrations in the system, is assumed to only have a detrimental effect on the real-time hybrid model test if the amplitudes are large enough or increase over time (Chabaud, 2016). This can only happen when an eigenmode of the system is excited, i.e. at resonance. Identification of the natural frequencies will be important. As mentioned, natural frequencies of the system should be filtered from the feedback signal to avoid amplification of the natural vibrations.

Impact hammer modal tests are done to identify natural frequencies of the system emulation (physical substructure connected to transmission system and motor). By use of a hammer, an impulse force is applied to the clock-spring or the physical mass that is attached to the transmission. In the frequency domain, an ideal impulse will include all frequencies, and by studying the impulse response one will find which frequencies are present in a system. Figure 10.3 shows power spectral density (PSD) estimates of the measured force from multiple hammer test. The plots are generated by giving hammer impulse loads to the clock-spring. The motor is disabled, and will not disturb the results.

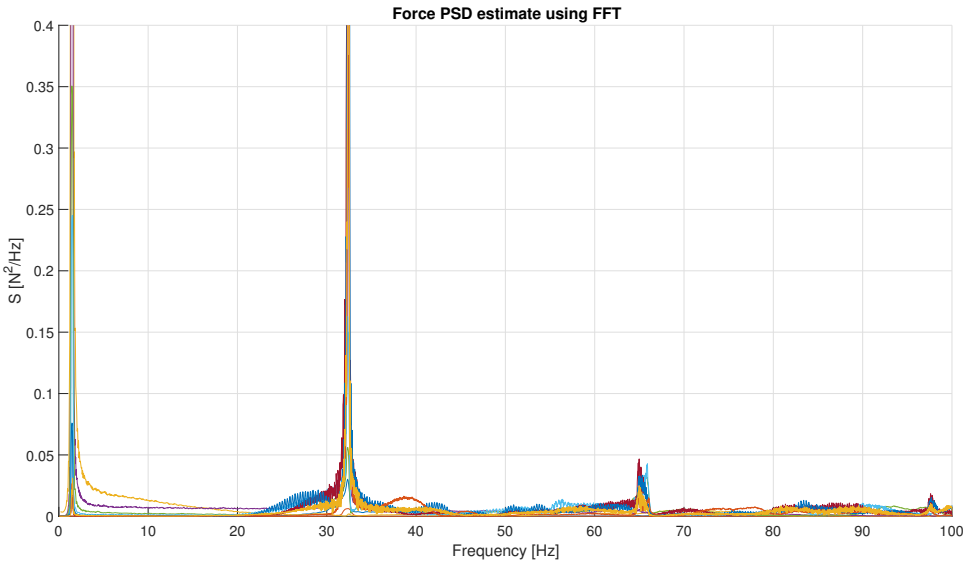

Figure 10.3: PSD estimates from hammer tests

From Figure 10.3 one can see that by giving impulse loads to the clock-spring, different frequencies

will give content to the measured force at the end of the wire. The clock-spring vibrations will excite transverse vibrations in the wire. At about 33 Hz, the fundamental wire vibration mode is probably found. The second mode is then seen at about 66 Hz, and the third mode at 99 Hz. In addition to the wire vibration frequencies, a large peak is found at about 1.5 Hz. A peak at the same frequency can be seen in Figure 10.4, which is generated by giving a hammer impulse load to the physical mass.

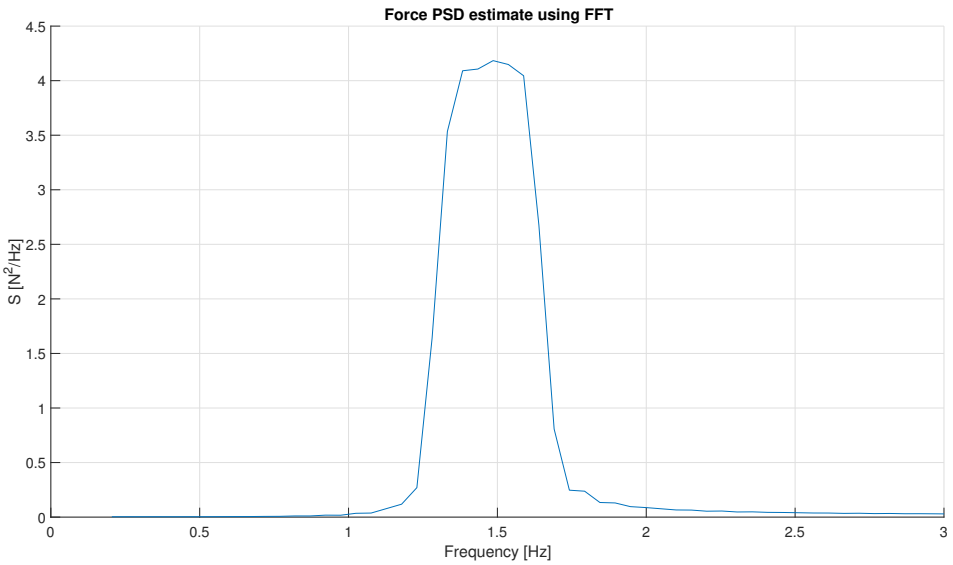

Figure 10.4: Coupled natural frequency

The peak at about 1.5 Hz corresponds to a coupled motion of the physical structure mass and the transmission. Due to a high stiffness of the wire, the physical structure and the wheel will oscillate together at the same frequency.

$$f_0 = \frac{1}{2\pi}\sqrt{\frac{k_P + k_s/r^2}{m_P + m_w}} \approx \frac{1}{2\pi}\sqrt{\frac{20 + 0.34/0.005^2}{1.84 + 0.15}} = 1.4 \text{ [Hz]}$$

The natural frequency of the stiff connection, depends on the physical structure mass, m_P, and wheel mass, m_w, the wheel radius, r, the clock-spring stiffness, k_s, and the physical structure stiffness, k_P.

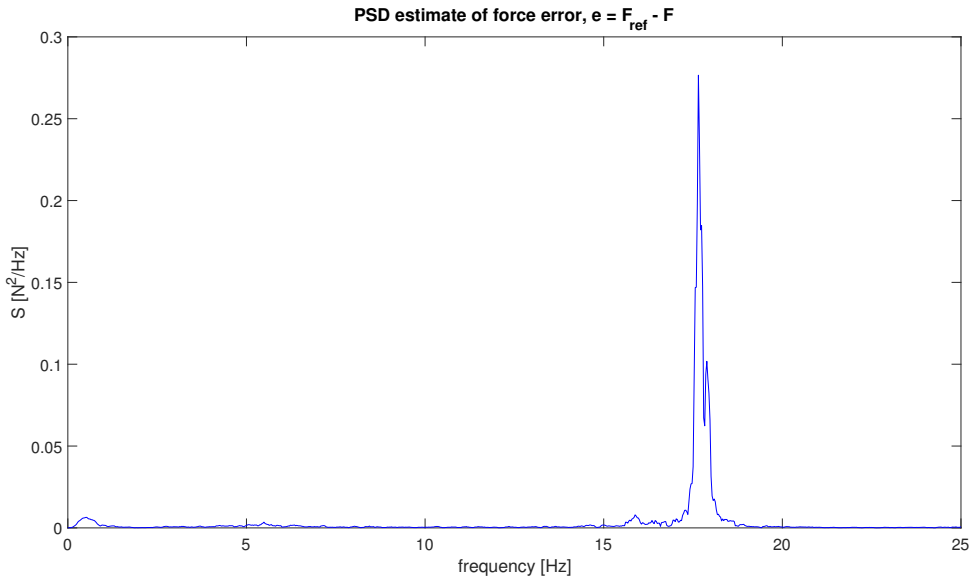

Figure 10.5: Wheel natural frequency

The decoupled dynamics of the wheel and physical structure can be seen from the force PSD plot in Figure 10.5. This plot is generated with the motor enabled, and with a force controller compensating for motions of the wheel. The wheel/clock-spring natural frequency is probably found at about 18 Hz, and the physical structure natural frequency at about 0.5 Hz (in this case the physical substructure has a natural frequency of 0.52 Hz).

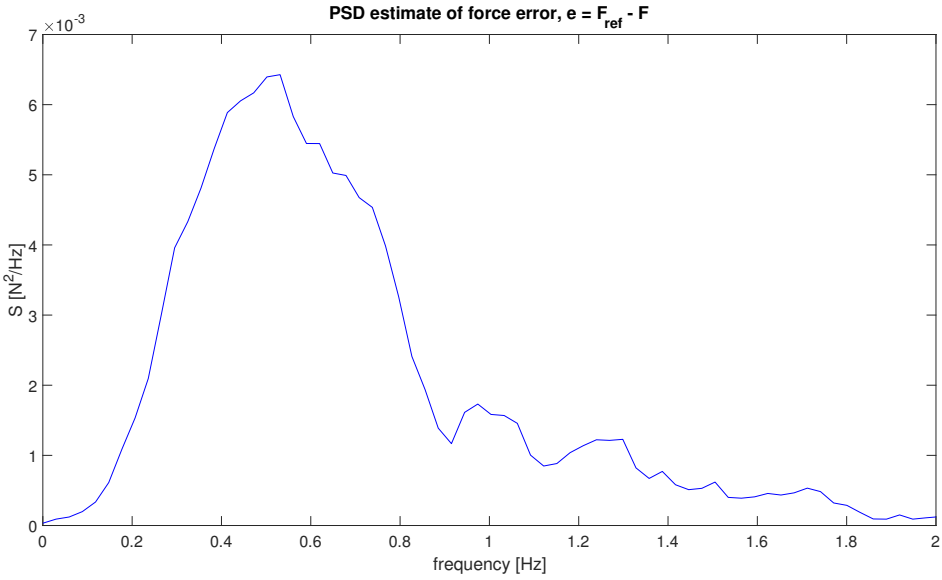

Figure 10.6: PSD estimate from hammer test

Figure 10.6 shows an enlargement of the peak corresponding to the physical structure natural frequency. This is the same peak as could be seen in Figure 10.5 for small frequencies.

10.5 Force observer

The need for a model-based filter that provides estimates of the applied force has been mentioned. A model-based filter (or observer) similar to the one used by Chabaud (2016) has been considered. It is given as a theoretical force, F_{th}, corrected by its lowpass filtered difference with the measurements, F:

$$F_{th} = \frac{k_s}{r}(\theta_M - \theta_w) \tag{10.2}$$

$$\hat{F}(s) = F_{th}(s) + L(s)\,(F(s) - F_{th}(s)) \tag{10.3}$$

k_s is the clock-spring stiffness, r is the radius of the wheel, θ_M is the motor angle and θ_w is the wheel angle. The so-called theoretical force, θ_{th}, is an analytic estimate of the force, based on the stiffness of the clock-spring and an angular deflection. As long as the angular positions, θ_M and θ_w, are correctly measured, this theoretical force should give a good indication of what the wire tension is. Even though it is a good estimate, the theoretical force does involve modelling errors and other uncertainties. The need for a correction based on measurements arise. The force measurements include high-frequancy measurement noise and process noise (in form of wire vibrations) that we want to exclude from the force estimate. A lowpass filter, $L(s)$, is used to filter out these frequencies. The lowpass filter will introduce a phase lag, but only on the unmodelled part of the force estimate.

Chapter 11

Uncertainties

11.1 Collocated vs. non-collocated control

Preumont (2011) looked at vibration control of active structures, and defined a collocated control system to be when the actuator and the sensor was attached to the same degree. Furthermore, it is not sufficient to be attached to the same location, but they also need to be dual. Dual means that the actuator and the sensor are connected such that the product of the actuator signal and the sensor signal represents the energy (or power) exchange between the structure and the control system. Collocated control then implies that a force-actuator must be associated with a translation sensor, which measures displacement, velocity or acceleration. A torque actuator needs then to be associated with a rotation sensor, measuring an angle or angular velocity. What has been referred to as the force-actuation system in this thesis, is actually a torque-actuation system. By measuring the wheel angle and controlling the motor angular position, a torque is applied to the wheel. Using knowledge of the wheel radius and a wire pulling the wheel, the torque-actuator is used to apply forces on a structure. By the definition of Preumont (2011), this torque-actuation system is collocated since it is associated with an encoder rotation sensor.

Chabaud (2016) had a non-collocated system. He used position of the physical mass as reference when controlling angular positions of the motor. Stiffness of the wire was thus included in the feed-forward control of forces. As long as the position of the wire attachment point is properly measured, this kind of control would not lead to major problems. The problems arise when this position is difficult to obtain. It could be that position of the physical structure is measured at one location, and the wire attached to a different location on the structure. Assuming that the structure is rigid, one could transform the measured position into a position of the wire attachment. By doing this assumption, the problems of non-collocated control could arise. Physical structures are seldom totally rigid, and such an assumption would lead to uncertainties, decreasing performance of a control system.

11.2 Wheel friction

Due to attachment of the encoder on the wheel, there will be some extra friction added to the wheel. The friction is assumed to be dependent on the encoder assembly pressure to the wheel. The effect of wheel friction will be analyzed next.

Open-loop force-tracking on moving mass

The effect of wheel friction can be seen in Figure 11.1, where the measured force is plotted against the reference force in open-loop control.

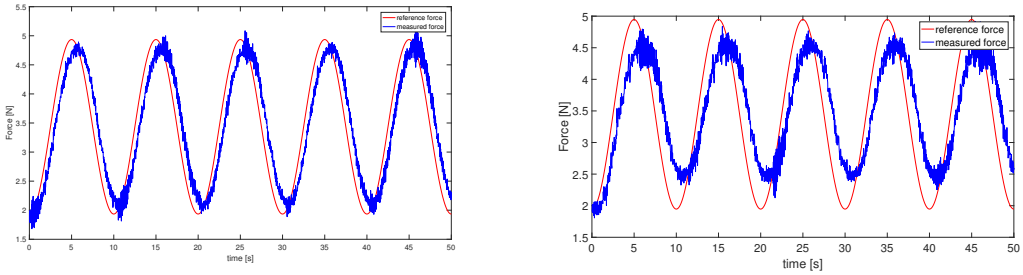

(a) Low encoder pressure

(b) Medium encoder pressure

Figure 11.1: Effect of wheel friction on force-tracking

Figure 11.1 shows that wheel friction decreases performance of the open-loop force control. The result is smaller amplitudes of the applied force, and a change of the sinusoidal shape. Due to friction, the peaks of the applied force gets flatter. The plots indicate that friction also adds a time delay to the system. This is obviously not the case, but the effect is seen because of a lag in the wheel motions. Figure 11.2 shows what is meant by lag in wheel motions.

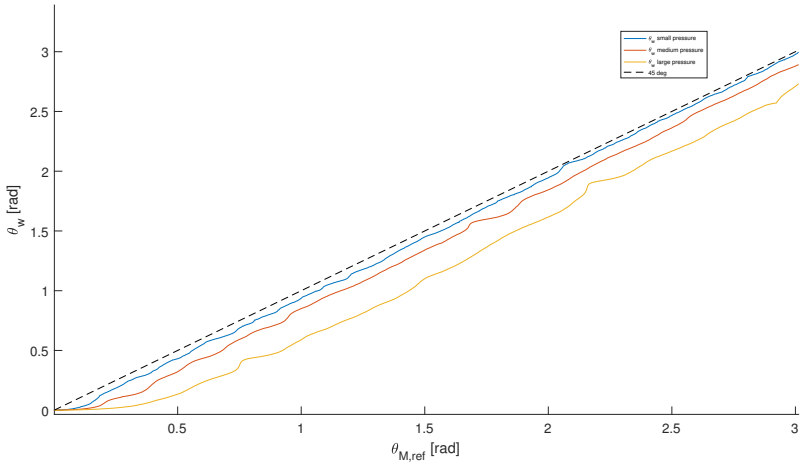

Figure 11.2: Mapping of angles

Figure 11.2 shows the measured wheel angle for a ramp input of the motor reference position. The wire is not connected, and the wheel moves freely. The plot is generated for different magnitudes of the encoder pressure on the wheel. One can see that as the motor angle changes linearly, the wheel angle does not follow exact. The wheel shows a less smooth motion with a lag compared to the motor. Friction is reason for this behaviour, and one can see that the effect is increasing with friction.

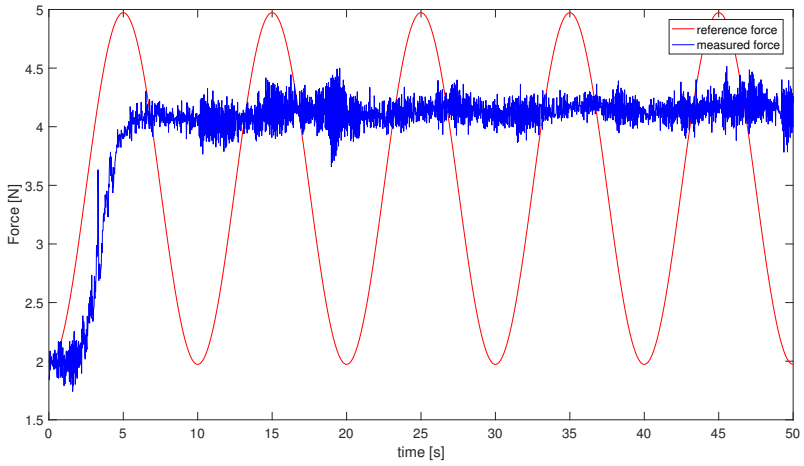

Figure 11.3: High encoder pressure

In Figure 11.3 one can see the effect of high friction due to high encoder pressure. If the friction is large enough, one can see that the wire may "feel" a constant force even though the motor, and the clock-spring torque, change. The motor position is controlled, and the clock-spring torque should change with sinusoidal shapes of 1.5 N amplitudes. Due to static friction, this oscillating clock-spring torque is not felt by the wire. After the wheel has found its equilibrium, the force ring measures an almost constant force of approximately 4 N. The force reference is given in the plot.

Decay test in following mode

Friction also has a clear effect on decay tests. If the wheel friction is high, the wheel will not reach its start position again after a decay test. One will see that the wheel finds an equilibrium with a steady state offset from the position it had before the decay test was carried out.

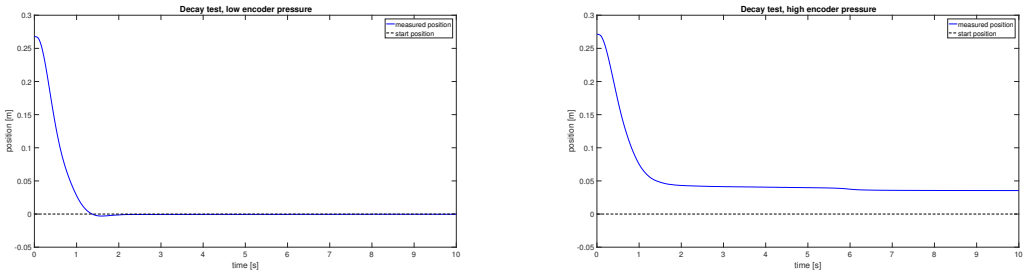

(a) Low encoder pressure

(b) High encoder pressure

Figure 11.4: Effect of wheel friction for decay test in following mode

In Figure 11.4, positions of the physical mass are plotted for two decay tests. Figure 11.4a shows a decay test of small encoder pressure, while Figure 11.4b shows a decay test of higher encoder pressure. One can see when the friction is high (i.e. high encoder pressure), the wheel finds an equilibrium with a steady state offset to the start position. In this case there is an offset of approximately 5 cm.

11.3 Encoder slipping

For some tests, the encoder measurement indicates slipping of the encoder/wheel connection. A slippery surface with some rough areas of the wheel is assumed to be reason for this drift in the encoder wheel angle measurements. The slipping will increase with smaller encoder pressure on the wheel, and since friction increases with higher encoder pressure, there will be a trade-off between wheel friction and encoder slipping. A solution to the problem could be: low encoder friction in combination with a bias estimate of the encoder slipping. Such a bias estimator is proposed next.

11.3.1 Bias estimate and position observer design

Using both the encoder and the ultra sound position sensor, two measurements of the wheel angle are available. The encoder provides a smooth and noise free measurement, but the problem of slipping has been addressed. The ultra sound position sensor provides drift-free measurements, polluted by measurement noise. A position observer, exploiting the advantages of both measurements is developed. Comparing encoder measurements with drift-free ultra sound measurements, the encoder slipping is estimated. By adding the estimated slipping to the encoder measurements, a wheel angle estimate is obtained.

In the succeeding derivations, the encoder slipping is referred to as a bias. The bias is given by:

$$b = \theta_w - \theta_e$$

where θ_w is the correct wheel angle, and θ_e is the encoder measurement. As in Fossen (2011), the bias

is modelled as a white noise driven process (i.e. the Wiener bias model).

$$\dot{b} = w_b$$

A Luenberg observer, estimating the bias is given by:

$$\dot{\hat{b}} = L(y - \hat{y}) \tag{11.1}$$

$$\hat{y} = \hat{b} \tag{11.2}$$

where $y = \theta_{us} - \theta_e$, and θ_{us} is the ultra sound measurement. By taking the Laplace transform of Equation (11.1), the bias estimator could be implemented as a first order transfer function:

$$\hat{b}(s) = \frac{L}{s+L} y(s)$$

As can be seen from the equations, the bias estimator is simply a lowpass filtered difference between drift free ultra sound measurements and the encoder measurements. Adding the estimated bias to the encoder measurements, a wheel angle estimate, $\hat{\theta}_w$, is given by:

$$\hat{\theta}_w = \theta_e + \hat{b}$$

Using an observer gain of $L = 0.1$, the performance of the wheel angle observer is plotted in Figure 11.5.

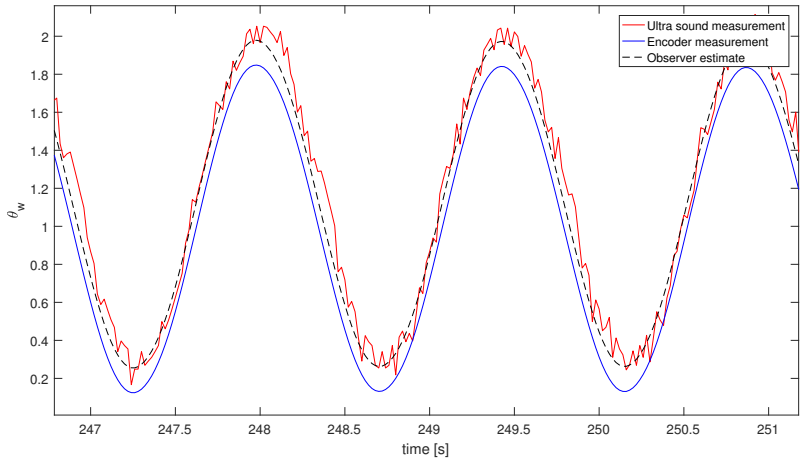

Figure 11.5: Bias estimate

Slipping of the encoder was not a problem in most tests. It seems like there is a certain area of the wheel that triggers slipping, and if that area is avoided, one will not see slipping. The bias estimator is not used in succeeding tests, but its derivations are included here to propose a solution to an observed and possible problem in the future.

Part IV

Validation of the force-actuation system, and 1-DOF real-time hybrid testing

Chapter 12

Validation of force-actuation system and sensitivity to parameter variations

Performance of the force-actuation system will depend on some key parameters. Important parameters includes: the predictor, the feedback controller gains, the force observer cut-off frequency, and the filter constant of the bias estimator. This chapter will present performance of the force-actuation system and an analysis of the predictor that was derived in Section 9.3.1. A sensitivity study of the experimental setup with regard to the predictor parameters will be carried out. The sensitivity analysis will be done in open-loop control, so that the feedback control does not affect the results. Analysis of the feedback controller and the force observer parameters are done by Truls Hamland. It is referred to Truls's MSc thesis for the choice of those parameters, and only one plot illustrating the use of feedback control will be given here. The bias estimator has not been used since slipping usually was not a problem.

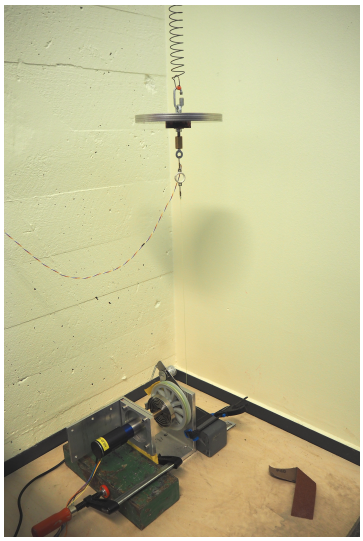

Figure 12.1: Experimental setup

12.1 Open-loop control

In open-loop, the force-controller has two inputs: the reference force, F_{ref}, and the wheel angle, θ_w. Analysis of both the force reference tracking part and the disturbance rejection part of the controller will be analyzed with respect to prediction.

12.1.1 Force-tracking on fixed mass

Force-tracking on a fixed mass, using the force-actuation system of Figure 12.1, is done to analyze performance of the force-tracking part of the force controller. The ability of the system to reject disturbances would then not influence the results, and it can be determined if the stiffness calibration and predictor parameters provide satisfactory mapping of the reference forces in open-loop. Due to time delay of the actuator and other system components, it will take some time before the reference force is mapped onto the physical structure. By predicting what the reference force will be forward in time, one can compensate for the delay. The predictor presented in Section 9.3.1 is used to extrapolate the force reference signal, F_{ref}. A third order polynomial is considered, since this order of the polynomial show best stability properties. Performance of the prediction will then be dependent on two key parameters: the extrapolation time, h, and the number of sample points, m, making the interpolation area. The amount of time one should extrapolate, will correspond to the time delay, and thus give an indication of the magnitude of this delay. The number of data points that are used to build the polynomial, will have a filtering effect. If the input signals to the predictor are noisy, the mean-square properties of the predictor will cancel some of this noise. Since the input signals in this case will be smooth, the m-number is assumed to be of less importance. An analysis has been done on this, but not included here (see Appendix C).

A parametric variation of the force reference prediction is done to analyze the effect of extrapolation time, h, for different input frequencies, f. The force mean-squared error (MSE) is chosen as key performance indicator (KPI).

$$KPI = MSE = \frac{\sum_{i=1}^{n} \left(F_{ref} - F\right)^2}{n} \tag{12.1}$$

Before calculating the force mean-squared error, high-frequency content is filtered from the measured force. This is done by a 4^{th} order Butterworth filter with cut-off frequency of 10 Hz. The high frequencies corresponds to measurement noise and natural vibrations in the transmission system, and filtering is done because we are only interested in the smaller frequencies of the applied force when analyzing the performance of the force prediction. Figure 12.2 shows power spectral density (PSD) plots of the measured force error. The high-frequency peak seen at 17 Hz, will be damped out

by the Butterworth filter.

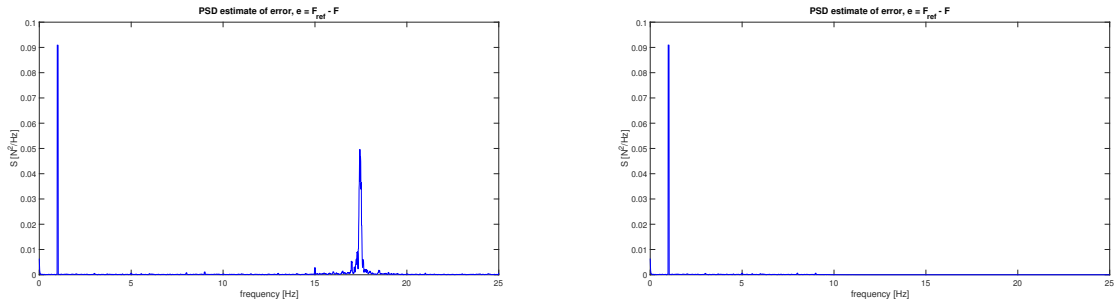

(a) Not filtered (b) Filtered

Figure 12.2: Force error spectrum

Table 12.1 shows a list of MSE values from force-tracking of a fixed mass. A selection of sinusoidal signals, covering the frequencies of interest, are sent as input to the force controller. The sinusoidal input signals has a magnitude of 1.5 N. The prediction polynomials are based on $m = 6$ sample points.

Table 12.1: MSE values for different input frequencies, f, and extrapolation times, h.

h/f	0,1 [Hz]	0,5 [Hz]	1 [Hz]	2 [Hz]	3 [Hz]
0,000 s	0,0029	0,0275	0,0979	0,3031	0,6390
0,010 s	0,0027	0,0434	0,0620	0,1836	0,3676
0,020 s	0,0026	0,0173	0,0336	0,0851	0,1470
0,030 s	0,0021	0,0057	0,0152	0,0346	0,0251
0,035 s	0,0020	0,0042	0,0089	0,0156	**0,0121**
0,040 s	0,0019	0,0026	0,0048	**0,0118**	0,0421
0,045 s	0,0018	0,0027	0,0025	0,0174	0,1200
0,050 s	**0,0017**	**0,0017**	**0,0017**	0,0374	0,2546
0,060 s	0,0019	0,0033	0,0106	0,1137	0,7014

The KPI values of Table 12.1 show that reference prediction enhance performance of the force-controller since time delays are compensated for. For all input frequencies MSE is largest for zero prediction. The MSE values decrease with extrapolation time up to a certain point, before they increase again. For each frequency, the smallest MSE value indicate the best performing extrapolation time. One can see that the low-points vary with frequency. It seems like an extrapolation time of 0.05 s performs best for low frequencies (0.1 Hz, 0,5 Hz and 1 Hz). For larger frequencies, the performance is better for smaller extrapolation times. A reference force of 2 Hz corresponds to a best performing extrapolation time of 0.04 s, and a reference of 3 Hz to an extrapolation time of 0.035 Hz.

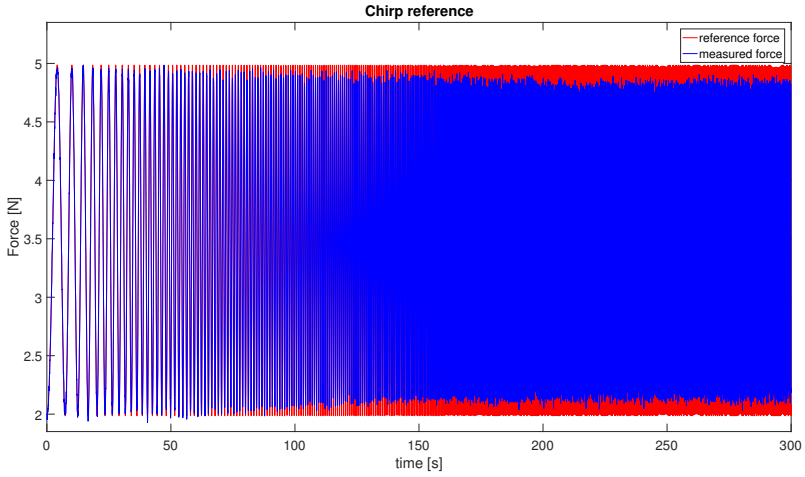

Figure 12.3: Force-tracking on fixed mass

Figure 12.3 shows the measured force plotted against a chirp reference force for force-tracking on fixed mass. The chirp reference includes frequencies from 0.1 Hz up to 3 Hz, in a time interval of 300 s. The controller command has been predicted 0.035 s ahead in time in the above test, to compensate for time delays. This extrapolation has been chosen for fixed-mass force-tracking because it shows good results for all frequencies of the chirp reference (see Table 12.1). It is not possible to see from the plot above if the measurements actually follow the reference, but one can observe that the amplitudes differ a bit for high frequencies. It looks like a lowpass filter effect, and could be due to the bandwidth of the motor.

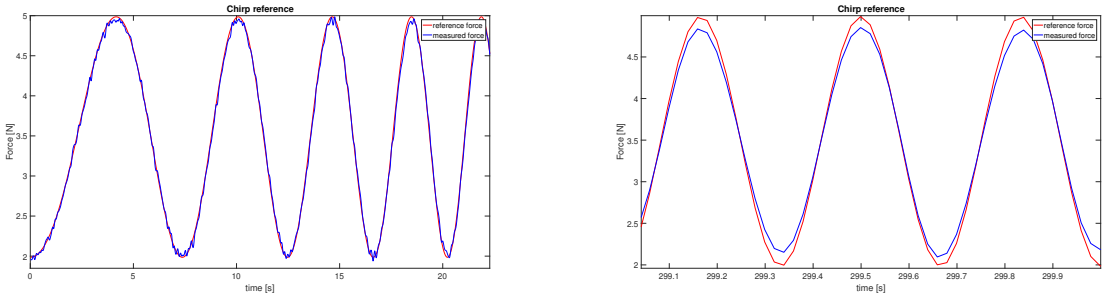

(a) Low frequencies

(b) High frequencies

Figure 12.4: Prediction by $h = 0.035$ s

In Figure 12.4, it has been zoomed in on the first part and the last part of the chirp plot in Figure 12.3. Figure 12.4a contains frequencies of 0.1 Hz and higher, and Figure 12.4b contains frequencies of 3 Hz and lower. One can see that the force-actuation system is able to apply forces of correct amplitudes for low frequencies. For higher frequencies, the force-actuator does not reach the amplitudes properly.

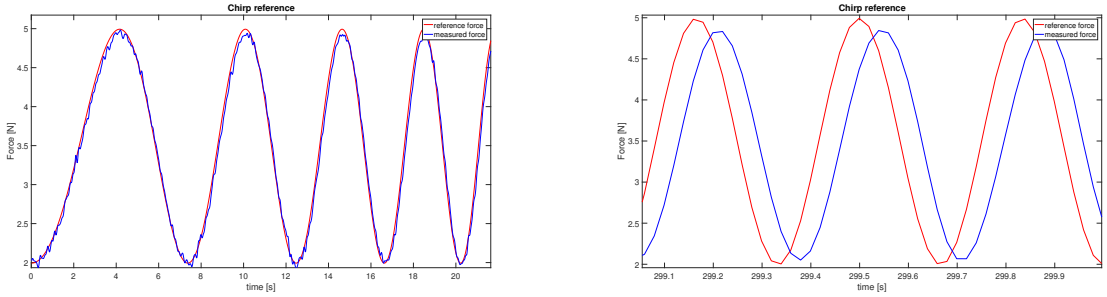

(a) Low frequencies (b) High frequencies

Figure 12.5: No reference prediction

Figure 12.5 shows a similar plot as 12.4, but is based on force-tracking without forward prediction of the reference. By comparing plots, we can see that the prediction works as it should. Table 12.1 indicates the same result. It is seen that the phase lag between reference and applied force is cancelled when predicting $h = 0.035$ s ahead in time.

12.1.2 Decay test in following mode

The effect of a predictor in the disturbance rejection part of the controller is analyzed by decay tests in following mode. Using the experimental setup depicted in Figure 12.1, the force-actuation system is asked to hold pretension, and the physical mass-spring-damper system is set in motion by releasing it away from equilibrium. A time delay will due to stiffness of the transmission, induce damping to the system. By predicting what the wheel angle will be forward in time, one can compensate for the time delay and reduce added damping. For larger extrapolation times, the accuracy of a polynomial prediction will be reduced. If the extrapolation times of the prediction are too large, it is expected that prediction lead to an unstable response. Just as for large negative phase lags, an over-prediction could leads to negative damping and instability.

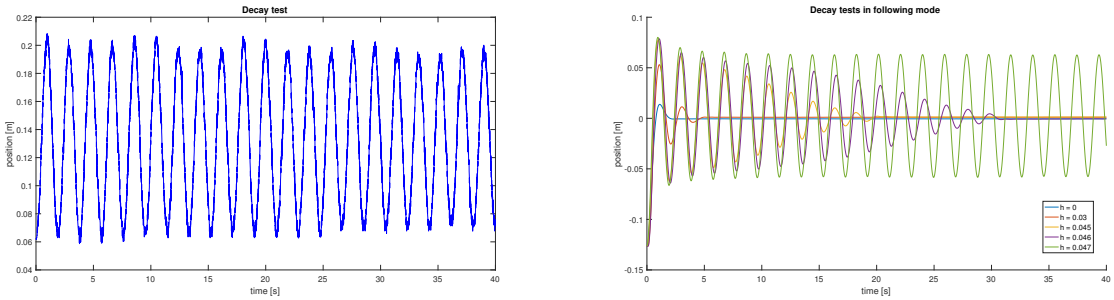

(a) Decay test without force-actuation system (b) Decay test in following mode

Figure 12.6: Decay test of physical structure with natural frequency $f_0 = 0.52$ [Hz]

Decay tests of a physical mass-spring-damper system with natural frequency $f_0 = 0.52$ Hz is considered. Figure 12.6a show a time-domain plot of a decay test with free oscillations. A small, but

positive damping can be seen from the plot. Comparing amplitudes of oscillations, a damping ratio of $\zeta = 0.0003$ is found for the physical substructure. Figure 12.6b presents decay tests of the same system, connected to the force-actuation system in open-loop following mode with 2 N pretension. One can easily see that by connecting the physical structure to the force-actuation system, additional damping is induced to the system. Prediction of the wheel angle, θ_w, will reduce this extra damping. The best results are observed with an extrapolation time of $h = 0.046$ s. As the extrapolation time is increased further, the system response turns unstable. An extrapolation time of $h = 0.047$ s seems to be a limit where the actuator induced damping goes from being positive to becoming slightly negative (i.e. the system gets unstable). Tests show that the system is very sensitive to time delays. A change in prediction of 1 ms is not much, but the change in response is significant.

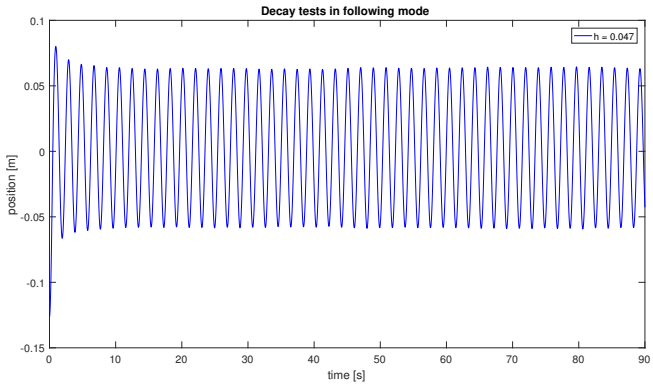

Figure 12.7: Prediction time $h = 0.047$

Figure 12.7 show the decay test with extrapolation time $h = 0.047$ s. When starting the system has a positive damping, but after some time it show a tendency of instability. At time 80 s, a damping ratio is calculated to be $\zeta = -0.0006$ by comparing amplitudes.

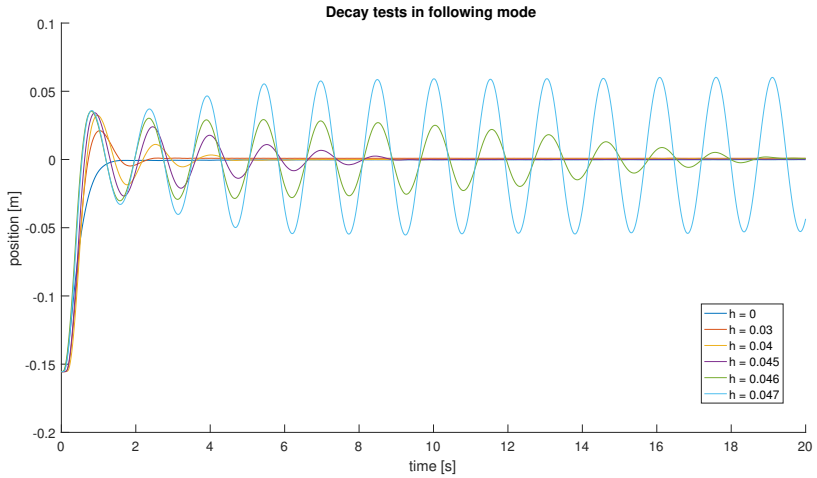

Figure 12.8: Decay test in following mode for system of natural frequency $f_0 = 0.71$ Hz.

Figure 12.8 show decay tests in following mode for a physical system of higher natural frequency. The system mass is reduced by 0.840 kg, making the natural frequency $f_0 = 0.71$ Hz. The effect of time delays are of even more importance for these high-frequency dynamics of smaller mass compared to the slower system of Figure 12.6. A discussion of sensitivity to delay will be given in Section 12.1.4. One can see that with no prediction, the system is overdamped. By predicting the wheel angle, the added damping is reduced. With an extrapolation time of $h = 0.047$ s, the system response is unstable. Best performance is obtained with an extrapolation time of $h = 0.046$ s, but the time delay induced damping is still prominent with that prediction. Like in the previous test, changes in extrapolation time of 1 ms show significant changes in response, and this makes tuning of the predictor difficult.

12.1.3 Force-tracking on moving mass

In real-time hybrid testing one is interested in applying reference forces on moving structures. Both the force-tracking properties and the disturbance rejection properties of the force controller will then be of importance. The succeeding results are based on controller command prediction, meaning that both the reference and the disturbance are predicted forward in time with equal prediction horizon, h. Forces are applied to a mass-spring-damper system of natural frequency $f_0 = 0.52$ Hz.

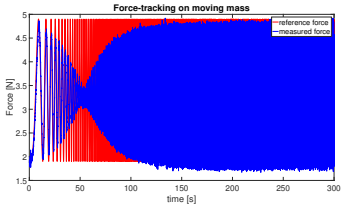

(a) $h = 0$ s

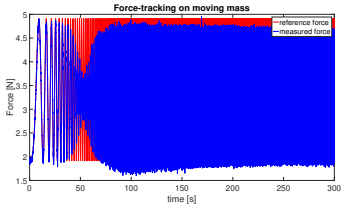

(b) $h = 0.035$ s

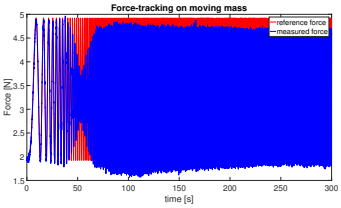

(c) $h = 0.046$ s

Figure 12.9: Chirp reference force-tracking with command prediction

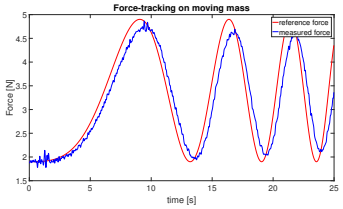

(a) $h = 0$ s

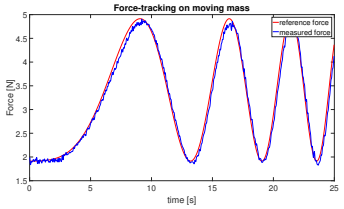

(b) $h = 0.035$ s

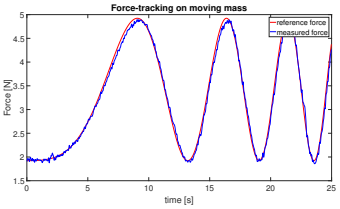

(c) $h = 0.046$ s

Figure 12.10: Low frequencies

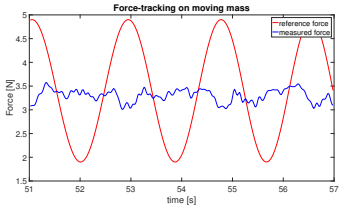

(a) $h = 0$ s

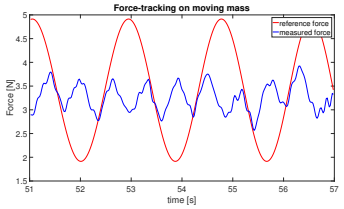

(b) $h = 0.035$ s

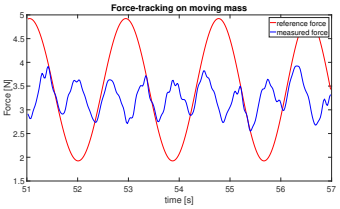

(c) $h = 0.046$ s

Figure 12.11: Natural frequency area

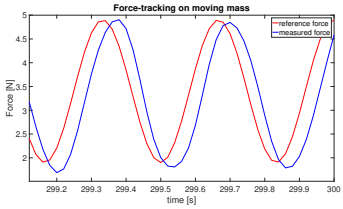

(a) $h = 0$ s

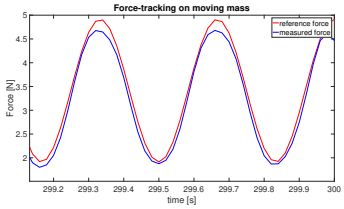

(b) $h = 0.035$ s

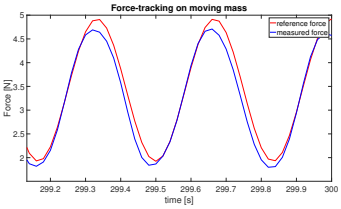

(c) $h = 0.046$ s

Figure 12.12: High frequencies

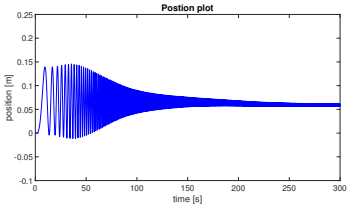

(a) $h = 0$ s

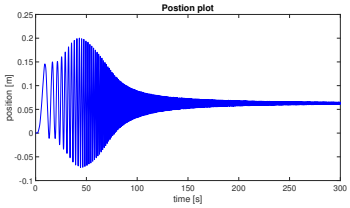

(b) $h = 0.035$ s

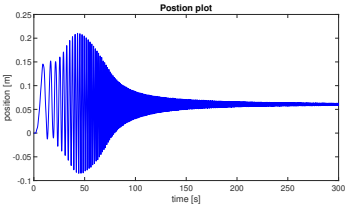

(c) $h = 0.046$ s

Figure 12.13: Position plot

Figure 12.9, 12.10, 12.11 and 12.12 show a chirp reference force plotted against the measured force for different lengths of the extrapolation time, h. The chirp reference signal include frequencies of 0.01 Hz up to 3 Hz, in a time interval of 300 s. Figure 12.13 show the measured position of the oscillating mass. It is clear that prediction has a positive effect on the force-controller performance for low frequencies. A command prediction will compensate for time delays when the reference frequencies are small. As the frequencies get higher, the controlled force is not able to follow the reference. A prediction of the controller command does not solve the problem when the system oscillates in its natural frequency, but from Figure 12.9 it seems like prediction has a positive effect, making the frequency area of large errors smaller (see the notch effect in figure).

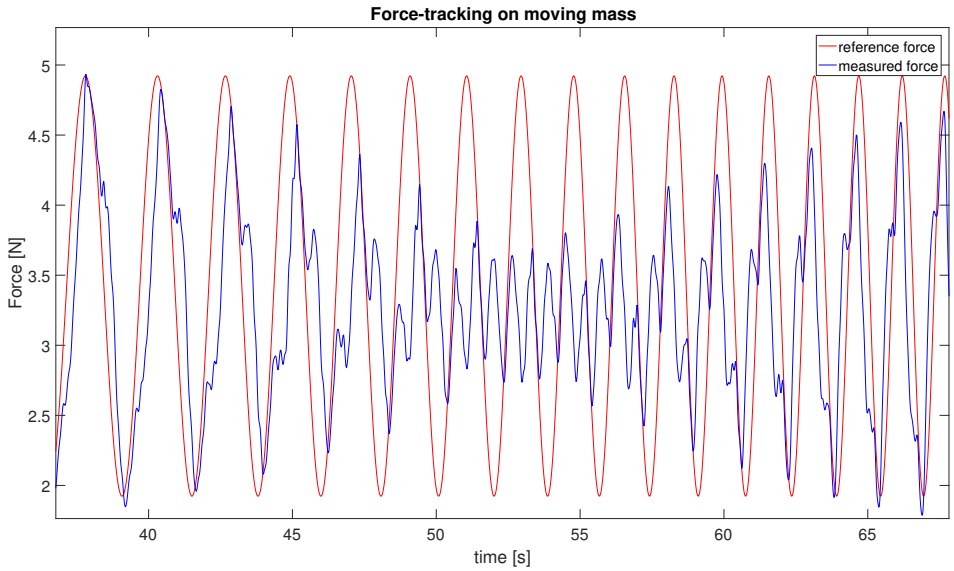

Figure 12.14: Natural frequency area, $h = 0.046$ s

Figure 12.14 shows the measured force plotted against the chirp reference in the natural frequency area of the moving mass. That is, when the chirp reference has a frequency of about 0.52 Hz. The reference has been predicted 0.046 s ahead in time to compensate for time delays. The measurements show a large error with the reference, and only small perturbations around a mean. It is seen from Figure 12.13 that also the amplitudes of oscillations are largest in the natural frequency area. It is hard to make conclusions on prediction in the natural frequency area of the system, as the applied force seems to be out of phase with the reference. It will be seen in Section 12.1.4 that it actually is the applied force error that is in phase with the reference. At higher frequencies, it seems like prediction has a positive effect again, cancelling a phase lag (see Figure 12.4b). Best performance for high frequencies seems to be with a prediction horizon of 0.035 Hz, which is in agreement with earlier observations done on fixed mass.

Another effect that is seen in Figure 12.14, is the forward-shift in time of the applied force com-

pared to the reference. The measurements have a phase lag compared to the reference. During the 30 seconds of the plot, one can see that the phase change from being negative to becoming positive. By closer inspection of plot 12.12a, the same forward shift can be seen for high frequencies. A first thought could be that the applied force lies more than a period behind the reference, but in Section 12.1.4 it is seen that a forward-shift in time probably is a better explanation.

Even with prediction, force-tracking on moving mass does not show satisfactory performance in the natural frequency area of the structure. However, prediction show good results for low frequencies. Realizing that validity of the force-actuation system has a frequency limit, prediction parameters for a smaller frequency interval are determined. Table 12.2 show the measured force MSE with the reference, for different frequencies of the reference. Time-domain plots are given on the next page for some of these tests.

Table 12.2: Sinusoidal reference force MSE

h/f	0,1 Hz	0,2 Hz	0,3 Hz	0,4 Hz
0,000 s	0,0750	0,2420	0,5210	0,9593
0,035 s	0,0157	0,0620	0,1436	0,5601
0,040 s	0,0122	0,0383	0,0823	0,5159
0,046 s	**0,0034**	0,0094	0,0236	0,6140
0,050 s	0,0048	**0,0088**	**0,0107**	0,3714
0,055 s	0,0198	0,0275	0,0145	**0,3238**

Table 12.2 indicates that prediction will be important for the force-actuation system performance at low frequencies. Figure 12.15, 12.16, 12.17 and 12.18 show the same results in time-domain plots. Extrapolation times between 0.046 s and 0.05 s give best performance for reference frequencies up to 0.3 Hz. For a reference frequency of 0.1 Hz, an extrapolation time of $h = 0.046$ s shows best performance. For 0.2 Hz and 0.3 Hz the best performance is obtained with $h = 0.05$ s. Performance of the force-actuation system is considerably reduced at 0.4 Hz. Prediction still helps at this higher frequency, and provides more correct amplitudes of the applied force. For $f = 0.4$ Hz the best performance is found at $h = 0.055$ s, but the time-domain plot shows tendencies to instability.

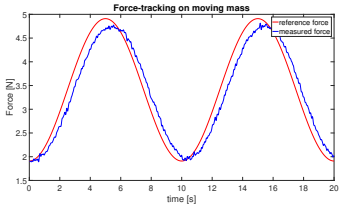

(a) $h = 0$ s

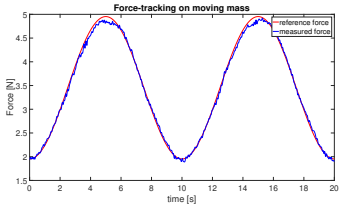

(b) $h = 0.046$ s

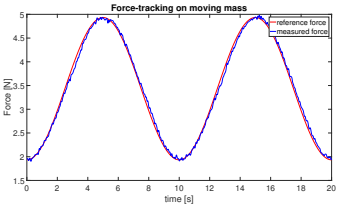

(c) $h = 0.05$ s

Figure 12.15: Reference frequency $f = 0.1$

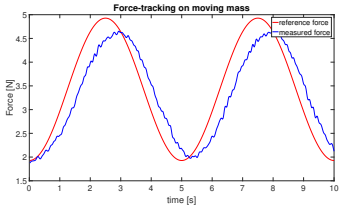

(a) $h = 0$ s

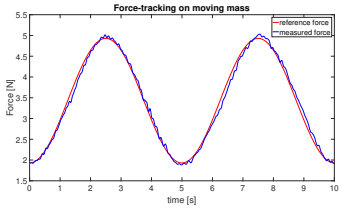

(b) $h = 0.046$ s

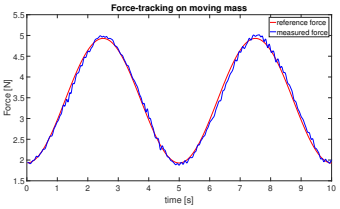

(c) $h = 0.05$ s

Figure 12.16: Reference frequency $f = 0.2$

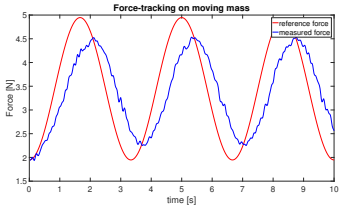

(a) $h = 0$ s

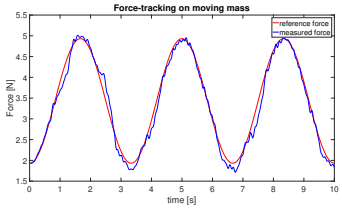

(b) $h = 0.046$ s

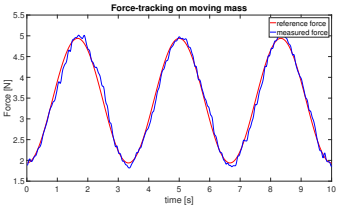

(c) $h = 0.05$ s

Figure 12.17: Reference frequency $f = 0.3$

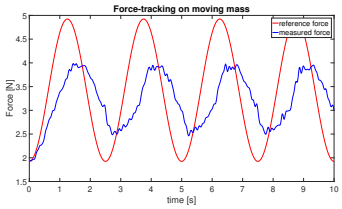

(a) $h = 0$ s

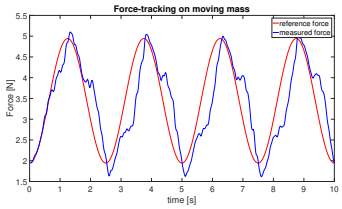

(b) $h = 0.046$ s

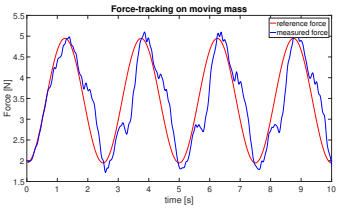

(c) $h = 0.05$ s

Figure 12.18: Reference frequency $f = 0.4$

12.1.4 Explaining observed effects

Large errors have been observed close to the natural frequency of the physical mass-spring-damper system. For small frequencies the applied force has a delay compared to the reference, and for large frequencies it seems like the phase lag is of more than a period or shifted forward in time.

To explain the observed effects, a simplified case of time-delayed force-tracking on an ideal mass-spring-damper system is considered. The delay is introduced in the disturbance rejection part of the force control, leading to a spring force due to stiffness of the clock-spring and the delay in rejection of disturbance, θ_w.

$$\begin{aligned} F &= F_{ref} - \frac{k_s}{r}\left(\theta_w(t) - \theta_w(t-h)\right) \\ &= F_{ref} - \frac{k_s}{r} h \frac{\theta_w(t) - \theta_w(t-h)}{h} \end{aligned}$$

The spring force will be determined by the clock-spring stiffness, k_s, the wheel radius, r, the time delay, h, and the delayed disturbance rejection error. Since the time delay will be of small magnitude, it can be seen as an added damping to the system

$$\begin{aligned} F &= F_{ref} - \frac{k_s}{r} h \lim_{h\to 0} \frac{\theta_w(t) - \theta_w(t-h)}{h} \\ &= F_{ref} - \frac{k_s}{r} h \dot{\theta_w} \\ &= F_{ref} - \frac{h k_s}{r^2} \dot{x} \end{aligned}$$

where the relation, $x = \frac{\theta_w}{r}$, has been used. The error of the applied force with the reference is then given by

$$e = F_{ref} - F = \frac{h k_s}{r^2} \dot{x} \tag{12.2}$$

Now, the frequency domain characteristics of the error is found by studying the frequency response of the physical mass-spring-damper system velocity, $\dot{x}$. The transfer function from applied force to output velocity is given by:

$$\frac{\dot{x}}{F}(s) = \frac{\frac{1}{m}s}{s^2 + 2\zeta\omega_0 s + \omega_0^2}$$

which has a Bode plot like Figure 12.19.

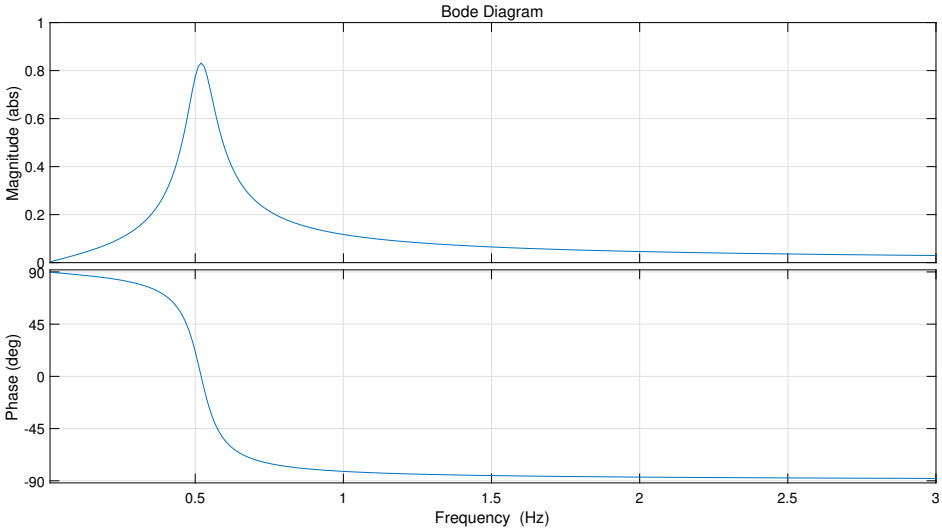

Figure 12.19: Bode plot of mass-spring-damper system velocity

Parameters of the real mass-spring-damper physical substructure has been used to generate the Bode plot of Figure 12.19. The Bode plot illustrates the transfer function from applied force to output velocity. Some extra damping is added to the system, this does not change any conclusions.

Table 12.3: Parameters of mass-spring-damper system

Parameter	m [kg]	f_0 [Hz]	ζ [-]
Value	1.840	0.52	0.1

The velocity response of the second order system is described by a magnitude gain and a phase compared to the input force. The Bode plot of Figure 12.19 indicate three characteristic areas of the velocity response: a stiffness dominated area, a resonance area and an inertia dominated area. The area of low frequencies, i.e when the input force is of lower frequency compared to the system natural frequency (0.52 Hz), is referred to as the stiffness dominated area. The stiffness dominated area is characterized by a low magnitude gain and a 90 degrees positive phase. When the input force has the same frequency as the natural frequency of the system, we are in the resonance area. The resonance area is characterized by a large magnitude gain peak and zero phase between applied force and output velocity. The area of high frequencies is referred to as the inertia dominated area, and is characterized by small magnitudes and a 90 degrees negative phase.

By Equation (12.2), the force error will have the same frequency characteristics as the velocity. A large error at the natural frequency is thus as expected. The fact that the error phase change from positive to negative at the natural frequency, is also seen in the phase plot of Figure 12.19. The applied

force is given by the reference subtracted by the error. For low frequencies the error lies 90 degrees in front, and is therefore subtracted from the reference. For high frequencies, it lies 90 degrees behind, and is thus added to the reference (due to the negative sign). This explains the forward shift of the applied force for high frequencies. Since the force error depends proportionally on the time delay, it is expected that the error should decrease with correct prediction. This is also in compliance with earlier observations and conclusions for the stiffness dominated and inertia dominated area of the response. In the resonance area prediction will result in smaller errors and less damping, which then again increase velocity and consequently the error. Unpredictable behaviour of the system at resonance can be understood.

It is seen that time delays induce an added damping to the system, and observations in Section 12.1.2 indicate that this extra damping had a more prominent effect when the mass of the physical structure was small. The effect can be understood by considering the induced damping factor, ζ.

$$\zeta = \frac{hk_s}{2r^2\omega_0 m} = \frac{hk_s}{2r^2\sqrt{km}} \tag{12.3}$$

It is seen from the above expression that the damping factor is increased with smaller mass. The time delay induced damping will thus be of more importance for smaller masses, as long as the stiffness is maintained the same. The result is a greater sensitivity to delays, and an increase in sensitivity to prediction.

12.2 Closed-loop force control

Tuning of the feedback loop is done by Truls Hamland. Closed-loop control has thus not been a concern to the author, but Figure 12.20 is included here to illustrate the effect of feedback control. At the time of writing this thesis, the feedback PID gains has not been determined. Better closed-loop controller performance is thus assumed to be obtainable.

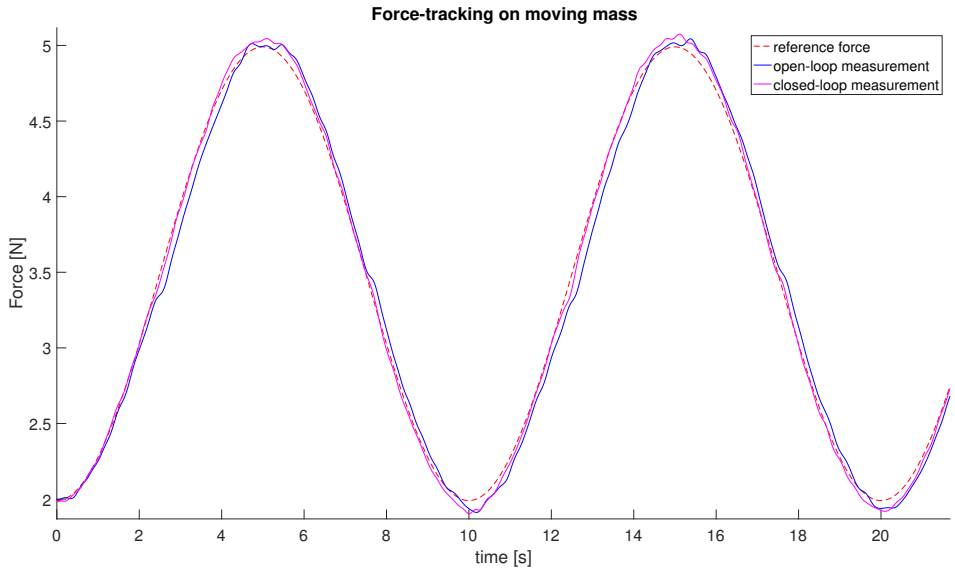

Figure 12.20: Closed-loop force-tracking on moving mass

Figure 12.20 shows the reference force plotted against measured open-loop and closed-loop controlled forces. The plots indicate better performance of the closed-loop control, where the feedback loop cancels an error in form of a phase lag. The observations agree with calculated MSEs. In open-loop the MSE is found to be 0.0093 N^2, while in closed-loop it is 0.0030 N^2.

12.3 Discussing the results

Open-loop force-tracking on a fixed mass approves the reference feedforward part of the controller. The clock-spring stiffness seems to be calibrated correctly, and by exploiting knowledge about the stiffness linearity we are able to apply forces of frequencies up to at least 3 Hz. At high frequencies the amplitudes are a bit reduced, probably due to the bandwidth of the actuator and a lowpass filter effect.

It was seen that low frequencies require more prediction, and the reason must probably be a difference in frequency and phase delay. It was mentioned in Section 9.3 that pure time delays and phase delays are lumped together and treated as one pure time delay when predicting. For low frequencies, ω, the equivalent pure time delays, h_{eq}, might therefore be large even though the phase delays are small (see Equation (12.4)).

$$h_{eq}(\omega) = h + \frac{\phi(\omega)}{\omega} \tag{12.4}$$

When trying to control forces on a moving mass, it is seen that the force-actuation system has limitations when it comes to rejecting (or following) motions of the structure it is connected to. Force-tracking on a moving mass show satisfactory performance only for a limited range of frequencies (up

to 3 Hz). When the motions become of large amplitude and velocity (i.e. at resonance oscillations), the system is unable to track forces on top of these motions. Reason for the error in applied force seems to be a delay in the disturbance rejection part of the control. A time delay in the disturbance rejection leads to an error proportional to the velocity of oscillations. As this error also increase with time delay, it is seen that compensation based on prediction has a positive effect when velocities are small. In the natural frequency area of the physical mass, it is difficult to make conclusions on the prediction. At resonance, a prediction will lead to less damping (and thus smaller error), which again leads to larger velocities that increase the error. For high frequencies, the amplitudes and velocities of oscillations becomes smaller, and the prediction has a more prominent positive effect again.

Performance of the force-actuation system could be enhance by the addition of a feedback control, as the feedback compensates for uncertainties in the open-loop control. An integral action of the feedback loop may improve the compensation of time delays. Performance of the feedback control is not considered by the author, and it is referred to the MSc thesis of Truls Hamland for analysis of the closed-loop controller performance.

12.3.1 Choice of predictor parameters

Observations show that prediction has a positive effect on the performance of the controlled force-actuation system for low frequencies. Extrapolation times between 0.046 s and 0.05 s shows best performance for force-tracking on a moving mass. Decay tests in following mode indicate instabilities for extrapolation times larger than 0.047 s. It is shown by force-tracking on moving mass that in the natural frequency area of the physical mass-spring-damper system, errors of the applied force with the reference are large. Also the amplitudes of oscillations are large in the natural frequency area of the system. For high frequencies, prediction show a positive effect again. An extrapolation time of about 0.035 s show good performance for high frequencies.

Realizing that validity of the force-actuation system has a frequency limit, forces of frequencies up to 0.3 Hz are considered within the bandwidth of the system. With these frequencies of interest, an extrapolation time of the predictor is chosen to be 0.46 s in further testing. The number of sampling points will be $m = 6$, as in previous tests. If noisy signals is a problem, more sampling points should be considered.

Chapter 13

Real-time hybrid test of coupled mass-spring-damper system

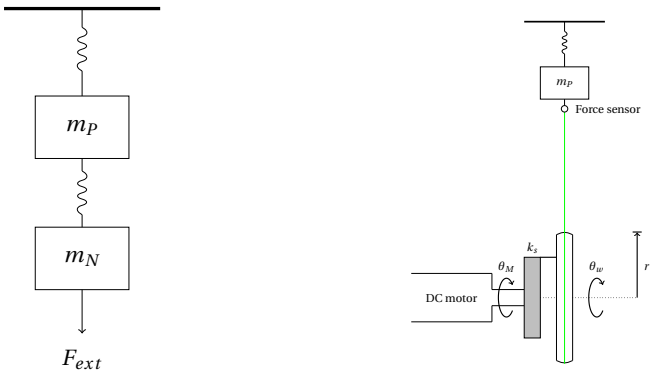

(a) System subject to testing

(b) System emulation

Figure 13.1: Test illustration

A force-actuation system has been developed, and its performance was analyzed in Chapter 12. The intention was to develop a system for use in force-based real-time hybrid model testing. This chapter will illustrate use of the developed force-actuation system in a real-time hybrid test. The system subject to testing was presented in Section 5.1 of the thesis, and is illustrated by Figure 13.1a. It consists of two connected mass-spring-damper systems, where the lower mass-spring-damper system and its external force is considered as the numerical substructure. A state-space model describing the numerical substructure dynamics was derived in Section 5.1, and given by Equation (5.1).

In a real-time hybrid test, the numerical substructure is replaced by an online simulation and an actuation interface (see Figure 13.1b). If the force-actuation system unable to apply requested forces of the simulation, the validity of the real-time test emulation is decreased. Analysis of Chapter 12 indicate that performance of the force-actuation system has a frequency limit of about 0.3 Hz. If the system subject to testing contains frequencies outside this bandwidth of the force-actuator, the real-

time hybrid test will be unable to reconstruct the responses of the system properly. In a valid test all frequencies must then be lower than 0.3 Hz, allowing the force-actuation system to compensate for or actuate all frequencies present in the system.

To evaluate the performance of the real-time hybrid test, a baseline system should be used as reference. With the springs at hand, a purely physical baseline system of frequencies lower than 0.3 Hz would result in a total system height of more than 5 m. An elastic spring is a longer spring, and lowering the elasticity or increasing the mass will both result in a larger system height. Restrictions when it comes to testing facility eliminate the idea of establishing such a physical baseline system. Instead a purely numerical baseline system is used as reference when studying responses of the real-time hybrid test. The test will then emulate a purely numerical system, and not a purely physical system which usually is the case. A fully numerical system of Figure 13.1a is developed in SIMULINK, providing great flexibility when it comes to system properties such as stiffness and mass.

System properties of what has been referred to as the physical substructure, will be the same as in previous tests (i.e. with natural frequency $f_0 = 0.52$ Hz). Ideally one would like smaller natural frequency of the physical substructure, but the test facility provides restrictions. However, tests will bring to light limitations of the real-time hybrid test due to inaccuracies in force-actuation. Parameters of both the physical and numerical substructure are given in Table 13.1 and Table 13.2, for two different test cases.

13.1 Comparing with SIMULINK baseline system

Validity of the real-time hybrid test is evaluated by comparing test results with the fully numerical model of system 13.1a developed in SIMULINK. The load case is described by a system initially at rest, with no external forces loading the system. A time $t = 0$ an external force of 3 N starts pulling the lower mass.

$$F_{ext}(t = 0) = 0 \text{ [N]} \tag{13.1}$$

$$F_{ext}(t > 0) = 3 \text{ [N]} \tag{13.2}$$

The load case is similar to a decay test, only that the equilibrium is changed instead of having moved the mass at start.

Case I

The first test case is described by a numerical substructure of natural frequency $f = 0.1$ Hz. The other system parameters are given in Table 13.1. The load case is given by Equation (13.1) and (13.2).

Table 13.1: Test parameters

Parameter	m_P [kg]	$f_{0,P}$ [Hz]	ζ_P [-]	m_N [kg]	$f_{0,N}$ [Hz]	ζ_N [-]
Value	1.840	0.526	0.0003	0.5	0.1	0.0020

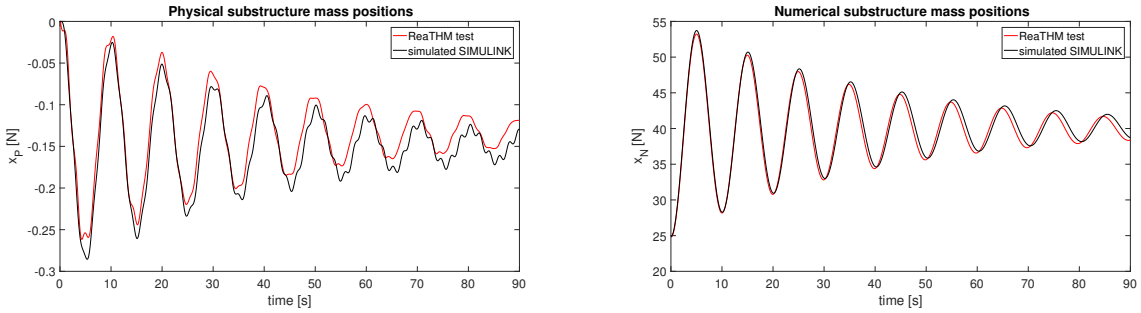

(a) Position of physical mass

(b) Position of numerical mass

Figure 13.2: Position plot

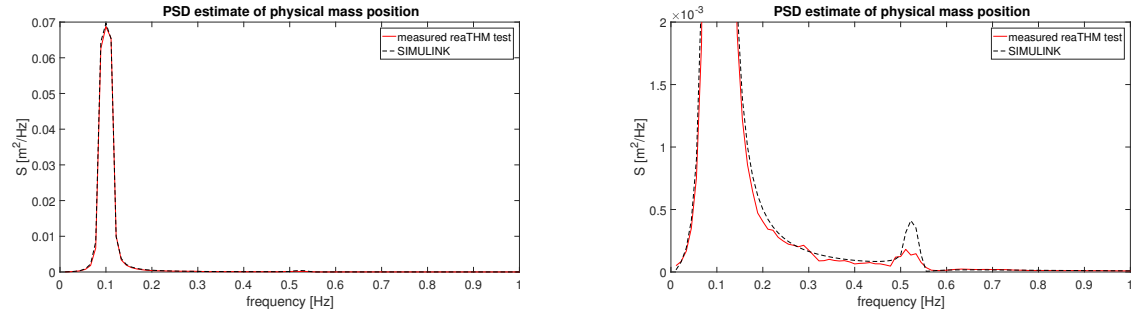

(a)

(b)

Figure 13.3: Physical mass position PSD estimates

Figure 13.2 shows the physical and numerical substructure responses of test case I. Measurements from the real-time hybrid test are plotted against simulations of the same system done in SIMULINK. One can see substructure motions that are not far from coinciding. The SIMULINK plot of Figure 13.2a shows a response containing more than one frequency. The effect of more than one frequency is less prominent from the real-time hybrid test. Figure 13.3 shows PSD estimates of the physical substructure mass position. Both the SIMULINK simulations and the real-time hybrid test show a large peak of equal height at 0.1 Hz. A smaller peak is found at about 0.52 Hz. The real-time hybrid test show a smaller peak compared to the SIMULINK simulations at this frequency.

Case II

In the second test case the numerical substructure has a natural frequency of $f = 0.2$ Hz. Other system parameters are the same as in case I, and given in Table 13.2.

Table 13.2: Test parameters

Parameter	m_P [kg]	$f_{0,P}$ [Hz]	ζ_P [-]	m_N [kg]	$f_{0,N}$ [Hz]	ζ_N [-]
Value	1.840	0.526	0.0003	0.5	0.2	0.0020

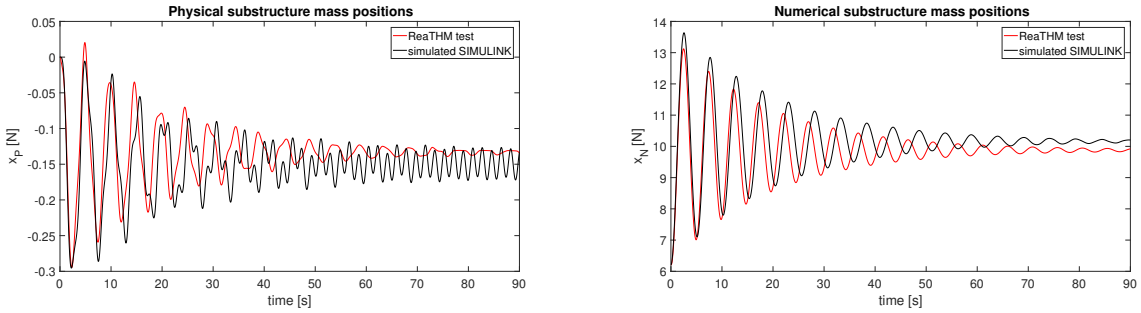

(a) Position of physical mass

(b) Position of numerical mass

Figure 13.4: Position plot

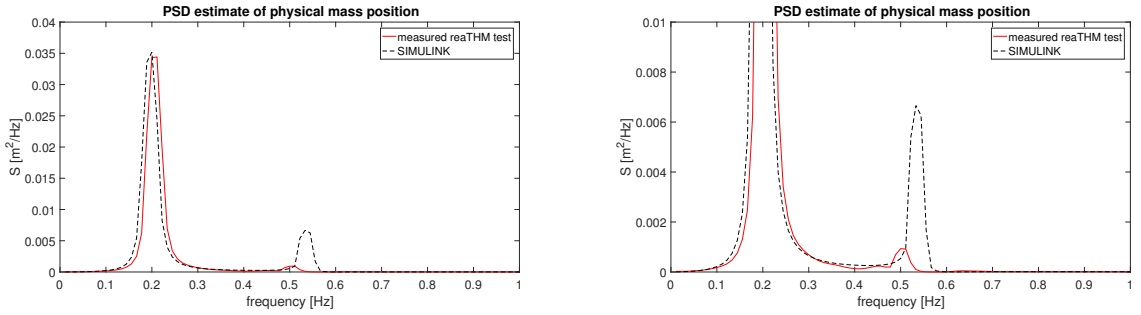

(a)

(b)

Figure 13.5: Physical mass position PSD estimates

Test case II shows a real-time hybrid test that is less equal to the SIMULINK simulations. The two tests shows much of the same substructure responses, but the effect of two frequencies in the system is much more prominent from the SIMULINK simulations. Both PSD plots of Figure13.5 shows a large peak at 0.2 Hz, and a smaller peak at 0.52 Hz. At 0.52 Hz the peak corresponding to the real-time hybrid test is much smaller than the peak from SIMULINK simulations. It is noticed that the 0.52 Hz peak is more prominent for test case II than it was for test case I.

13.1.1 Discussing validity of the real-time hybrid test

In test case I the real-time hybrid test imitates the fully numerical model quite well despite limitations of the force-actuation system. Tests show substructure responses that are not far from coinciding, and reason is that the response is dominated by the 0.1 Hz frequency. Limitations of the real-time hybrid test are most prominent in the PSD plots. The PSD plots indicate that the natural frequency motions

of the physical substructure are damped out in the real-time hybrid test, and closer inspection of the time-domain plots leads to the same conclusion. The results are as expected. It was observed in Chapter 12 that the force-actuation system is unable to suppress these natural frequency disturbances properly, and the results presented here amount to the same conclusion.

Test case II show a real-time hybrid test response that is less equal to that of the baseline SIMULINK system. Since the two substructures in case II are of more equal natural frequency, closer to what has been determined as a frequency limit of the force-actuator, it is expected that the physical substructure response will be more dominant in the coupled dynamics response. The result is a worsening of the real-time hybrid test emulation.

Chapter 14

Conclusions

14.1 Concluding remarks

A force-actuation system has been developed, and challenges related to the mapping of reference forces on moving structures have been clarified. Time delays, noise and uncertainties in the system are mentioned problems. The observed time delays are significant, and these have been the main challenge in the development of a valid force-actuation system.

The feedforward mapping of reference forces works as it should. Utilizing the linear stiffness properties of a clock-spring and an angular deflection, we are able to track forces of requested frequencies on structures at rest. Problems arise when the physical structure, on which we want to apply forces, starts to move. Time delays will then challenge the feedforward rejection of disturbances, and lead to inaccurate force-tracking on structures in motion. Errors due to time delays increase with the amount of delay and the disturbance velocity. By disturbances we mean motions of the physical structure that the force-actuation system is connected to and applies forces on. For small velocities, compensation by polynomial prediction reduce the problem of time delays. When the moving structure moves at high velocities, e.g. when it is excited at its natural frequency, the force-actuation system is not able to suppress disturbances and control forces on the moving structure.

If the force-actuation system is not able to reconstruct all frequencies in a real-time hybrid test properly, the test emulation will not be valid.

14.2 Suggestions to further work

Time delays have been a problem. One could try to reduce the amount of delay in the system. A more effective code, allowing smaller sampling period is suggested. The LabVIEW code is now programmed in hybrid mode (using both scan engine and FPGA). It is expected that a code programmed in FPGA exclusively would be a more effective code. For further work, it is suggested to use a different motor. The FAULHABER DC-servomotor currently in use shows large time delays that make the development of a valid force-actuation system difficult. It is recommended to use a faster servomotor to provide smaller time delays.

The force-controller, force-observer and predictor currently in use are exceedingly simple. Model-based strategies may enhance performance of the system, and this is suggested for further work.

A different encoder assembly is possible. By letting the encoder for example rotate with the wheel shaft, friction of the wheel could be reduced. This would avoid possible problems with slipping of the encoder.

When a force-actuation system of acceptable performance is obtained, a more complex real-time hybrid test could be carried out. A system of two or three degrees of freedom would be more similar to real applications. This will require implementation of additional components to the hybrid test loop. A force-allocation algorithm would for example be needed.

Part V

Appendices

Appendix A

System identification

A.1 Physical substructure model

The dynamics of the physical substructure, can be described by three parameters: the mass m_P, the damping b_P and the stiffness k_P of the mass-spring-damper system. While the mass is easily measured, the damping and stiffness is usually found from studying free oscillations.

$$\ddot{x} + 2\zeta_P \omega_0 \ddot{x} + \omega_0^2 x = 0 \tag{A.1}$$

Lets look at the normalized second order homogeneous ODE (A.1), describing the free oscillation dynamics in terms of the damping ratio ζ_P and natural frequency ω_0. In the time domain, a solution to the differential equation is found by looking at the roots of the characteristic equation:

$$\lambda_{1,2} = -\zeta_P \omega_0 \pm i\omega_0 \sqrt{1-\zeta_P}$$

The general solution is:

$$x(t) = Ae^{-\zeta_P \omega_0 t} sin\left(\omega_d t - \phi\right)$$

where $\omega_d = \sqrt{1-\zeta_P}\omega_0$ is the damped natural frequency of the system.

Since the system is underdamped, the values of ζ_P and ω_0 can be found by analyzing the response to an initial displacement of the mass. The peak frequency of the response spectra corresponds to the damped natural frequency, ω_d. Then, by looking at the ratio of x at two succeeding maxima, one is able to determine ζ_P and ω_0.

$$\frac{A_1}{A_2} = \frac{Ae^{-\zeta_P \omega_0 t_1}}{Ae^{-\zeta_P \omega_0 t_2}} \quad \Rightarrow \quad -\zeta_P \omega_0 (t_1 - t_2) = ln\left(\frac{A_1}{A_2}\right) \tag{A.2}$$

The dynamics of the physical substructure, is easily changed by adjusting one or more of the system components. Table A.1 list some system parameters that are used in testing of the real-time hybrid

test setup. The mass is changed to adjust the natural frequency of the system, while the spring is left unaltered.

m_P [kg]	ζ_P [-]	f_0 [Hz]
1.840	0.0003	0.52
1	0.0003	0.71

Table A.1

Figure A.1 show an example of a response power spectrum, for a mass-spring-damper system with natural frequency of 0.6 Hz.

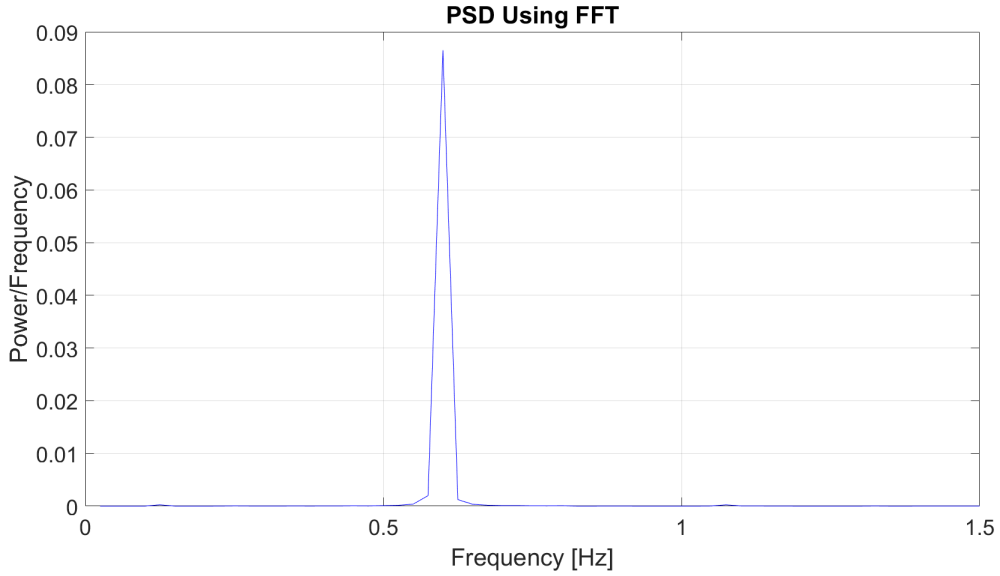

Figure A.1: Power spectrum of the physical substructure harmonic oscillations

The normalized system parameters, ζ_P and ω_0, can be used to obtain the damping and spring coefficients of the physical substructure (the mass-spring-damper system):

$$k_P = \omega_0^2 m_P, \quad b_P = 2\zeta_P \omega_0$$

Appendix B

Motor data

DC-servomotor specifications

Table B.1: DC Servomotor key technical data, ref (DC Motor Spesifications).

Symbol	Description	Value	Unit
T_{max}	Recommended torque up to	44.0	mNm
b	Motor viscous friction constant	$2.3 \cdot 10^{-6}$	$Nm/(rad/s)$
K	Back emf constant	0.0201	$V/(rad/s)$
R	Armature resistance	1.2	Ω
J	Rotor inertia	$3.4 \cdot 10^{-6}$	kgm^2
L	Armature inductance	$194 \cdot 10^{-6}$	H

Gearhead specifications

Table B.2: Precision gearhead technical data, ref. (Gear Specifications)

Symbol	Description	Value	Unit
-	Reduction ratio	43:1	-
η	Efficiency, max	70	%

Motion controller ASCII commands

Table B.3: Motion control ASCII commands

Command	**Function**	**Description**
EN	Enable Motor	Activate drive.
DI	Disable Motor	Deactivate drive.
LA	Load Actual Position	Load new absolute target position relative to home position.
LR	Loads Relative Position	Load new relative target position, in relation to last started target position.
M	Initiate Motion	Activate position control and start positioning.
HO	Define Home Position	Defines Home Position. Without argument: set actual position as 0.

Appendix C

Additional results

C.1 Analyzing effect of sample number, m

Table C.1: List of KPI values for different combinations of predictor parameters. The KPI values are of unit $[N^2]$. The frequency of the force reference is: f = 0.5 [Hz]

h/m	10	20	25	30	40
0	0,0304	0,0317	0,0308	0,0298	0,0258
0,01	0,0205	0,0211	0,0208	0,0195	0,0163
0,02	0,0129	0,0167	0,0135	0,0120	0,0091
0,03	0,0069	0,0085	0,0072	0,0072	0,0050
0,04	0,0037	0,0044	0,0039	0,0042	**0,0036**
0,05	**0,0037**	**0,0035**	**0,0028**	**0,0039**	0,0055
0,06	0,0037	0,0040	0,0045	0,0061	0,0113
0,07	0,0064	0,0074	0,0087	0,0119	0,0200

The table show a list of KPI values for force-tracking on fixed mass. The force reference has a frequency of $f = 0.5$ Hz. It is seen that best performance is obtained for the same extrapolation time, h, for all of the lower sample points, m. The highest number of sample points show best performance for a lower extrapolation time.

Bibliography

Carrion, J. E. and Spencer, B. F. (2007). Model-based Strategies for Real-time Hybrid Testing. (December):211.

Chabaud, V. (2016). Real-Time Hybrid Model Testing of Floating Wind Turbines.

Chen, C.-T. (2014). *Linear system theory and design*. Oxford University Press, New York, 4th international edition, Reading, Massachusetts.

Fossen, T. I. (2011). *Handbook of Marine Craft Hydrodynamics and Motion Control*. Wiley.

Jens G. Balchen, Trond Andresen, B. A. F. (2003). *Reguleringsteknikk*. NTNU-trykk.

Kreyszig, E. (2011). *Advanced Engineering Mathematics*. Wiley.

Plummer, A. (2006). Model-in-the-Loop Testing. *Proceedings of the Institution of Mechanical Engineers, Part I: Journal of Systems and Control Engineering*, 220(December):183–199.

Preumont, a. (2011). *Vibration Control of Active Structures*, volume 179.

Robert Grover Brown, P. Y. H. (2012). *Random Signals and Applied Kalmen Filtering*. Wiley.